Journal of Constructional Steel Research 188 (2022) 107014

Contents lists available at ScienceDirect

Journal of Constructional Steel Research

journal homepage: www.elsevier.com/locate/jcsr

Elimination of intermediate stiffeners in box link beam using low yield point steel

Danial Pesaran Behbahani, Nader Fanaie *

Department of Civil Engineering, K. N. Toosi University of technology, Tehran, Iran

ARTICLE INFO

Keywords:
Eccentrically braced frame (EBF)
Box link beam
Intermediate stiffener
Low yield point steel
Finite element method

ABSTRACT

The use of intermediate stiffeners in the link beam, in addition to increasing the cost of construction and reducing the speed of execution due to the need to welding operations, can lead to residual stresses. In this study, in order to remove the intermediate stiffeners in box link beam, the idea of using two types of low yield point steel (made in Japan and China) in the web of box link beam has been investigated using the finite element modeling in Abaqus software. According to this study, using low yield point steel in link beam without intermediate stiffeners, the maximum permissible compactness ratio of link web can be considered up to 56% greater than the maximum compactness ratio provided for common structural steels. The overstrength factor for the two types of low yield point steel made in Japan and China is calculated as 4.14 and 2.58 on average, respectively, while the value of this parameter proposed in accordance with AISC seismic provisions for box link beams made of common structural steels is 1.4. Using low yield point steel in the link beam and eliminating the intermediate stiffeners, the energy dissipation of the link beam can be increased to about 30% and its elastic stiffness can be increased to about 45%. In addition, by using low yield point steel and elimination of the intermediate stiffeners, undesirable fracture mode in the vicinity of the stiffeners is removed, and the rotation limit corresponding to fracture of the link beam increases to about 85%.

1. Introduction

The input energy caused by the earthquake to the structures, according to the law of conservation of energy, is converted into kinetic energy, elastic strain energy, viscous energy, and nonlinear strain energy (hysteretic energy). In the common structures in the face of severe earthquakes, about 90% of the input energy to the structure is dissipated by the hysteretic energy [1]. The use of energy absorbent members was suggested in order to concentrate the hystertic energy dissipation and consequently to damage the structure, in a special area that is suitable for energy dissipation (structural fuse). Passive energy dissipation has been used since the 1980s to control the structure vibrations. In the passive energy absorbing system, the members of the energy absorber are installed to improve damping, stiffness, and strength in the structure. Of the types of passive dampers in the structure is the metallic yield dampers that dissipate the input energy from the earthquake through the response of hysteretic cycles and consequently prevent damage to other members of the structure. The use of metal dampers, due to their easy production, specific response, and stable mechanical performance is popular among energy dissipation methods. In the early 1970s, new structural system called eccentrically braced system was created in Japan, with the same logic as passive yield dampers, and then in the United States, this type of system was investigated by Popov et al. since 1978. In this lateral force resisting system, non-elastic behavior and energy dissipation is restricted to a specific area called link beam, and other frame members must necessarily behave linearly and elastically. Eccentrically braced frame is a combination of suitable lateral stiffness of concentrically braced frame and proper ductility of moment resisting frame. The lateral stiffness of the eccentrically braced frame is less than that of the concentrically braced frame, but in the concentrically braced frame, early buckling of the braces in the earthquake reduces the lateral stiffness of the frame while in the eccentrically braced frame the possibility of buckling is not given to the braces so that the stable behavior of the structure is guaranteed. Behavior of eccentrically braced frame depends greatly on the behavior of the link beam, in other words, the link beam function like fuse, which with their ductile behavior, firstly provide energy dissipation and response modification factor in the seismic lateral force resisting systems, and secondly limit the efforts of other members of the frame. The short link beam by dissipating energy from

* Corresponding author at.: K. N. Toosi University of Technology, Civil Engineering Department, No. 1346, Vali-Asr Street, P.O. Box. 15875-4416, 19697 Tehran, Iran.
E-mail address: fanaie@kntu.ac.ir (N. Fanaie).

https://doi.org/10.1016/j.jcsr.2021.107014
Received 20 August 2021; Received in revised form 18 October 2021; Accepted 23 October 2021
Available online 10 November 2021

Nomenclature

τ_{cr}	The critical shear buckling stress of the plate
$k(\alpha)$	The constant which is subject to the boundary conditions of the plate and its aspect ratio (α)
D	The flexural elastic stiffness of the plate
t	Thickness of plate
ϑ	The Poisson's ratio of the steel
β	The compactness ratio of the plate
b_f'	The pure width of the flange regardless of the thickness of the webs
d'	The depth of the web regardless of the thickness of the flanges
t_f	The thickness of the flange
E	The modulus of elasticity
F_{yw}	The yield stress of the web
F_{yf}	The yield stress of the flange
a	The distance from center to center of stiffeners
d	Depth of beam
t_w	Thickness of the web
γ_u	The expected ultimate rotation in the link beam
F_{uw}	The ultimate stress of the web materials
F_{yst}	The yield stress of stiffener materials
A_{st}	The stiffener area
σ^0	The size of yield surface
α_k	The Kth backstress, which represents the location of the center of yield surface
C_k	Initial kinematic strain hardening slope
γ_k	The rate of reduction of the kinematic hardening slope
ε^p	Plastic strain
a_0^k	The initial size of the backstress
$\sigma\|_0$	The initial size of yield surface
σ_∞^0	The maximum change in the size of the yield surface
ε_{eq}^p	The equivalent plastic strain
V_u	The shear force induced due to Design Based Earthquake in link beam (Eq. (13)) or is the maximum shear created in the link beam (Eq. (25))
V_n	The nominal shear capacity in link beam
$\varnothing$	The strength reduction factor
A_w	The net web area
M_P	The cross-section plastic moment
M_{Pf}	The flange plastic moment
M_{Pw}	The web plastic moment
V_f	Flange contribution in the plastic shear capacity of the box link beam
e	The length of link beam
b	The width of the flange in the link beam
I_b	The moment of inertia of the link beam
G	The shear modulus
L	The span length of the frame
$\frac{\Delta_i}{h}$	The interstorey drift ratio of the floor
R	The radius of spherical void
σ_m	The hydrostatic stress
σ_e	The von-Mises effective stress
R_0	The initial radius of the void
A	The material constant
η	Stress triaxiality
A_R	The reduction of the cross-section of the sample at the fracture zone in the tensile test on uniaxial axisymmetric tensile specimen

link's shear yield, behaves much better in terms of elastic lateral stiffness, ductility, energy dissipation, and ultimate lateral strength than longer link beams [2]. In general, if the ratio of the link beam length (e) to the length of the braced span (L) is more than 0.5, the lateral stiffness of the eccentrically braced frame is not much different from the moment resisting frame. According to the aforementioned points, in this study, the eccentrically braced frame with short link beam has been investigated. It is worth noting that if the length of the link beam is considered too short, its non-elastic rotation will increase. In order to prevent the complete destruction of slab concrete in the upper part of the link beam in the eccentrically braced frame, the AISC 341–16 [3] limits the maximum non-elastic rotation in the short link beam to 0.08 rads, thus limiting the minimum permitted length of the link beam. A variety of eccentrically braced frame is displayed in Fig. 1 [4].

In investigating the behavior of shear link beam without intermediate stiffeners in cyclic loading, it has been found that due to early shear buckling in the link's web, stiffness and strength degradation, and consequently, reduction of energy dissipation is observed in the sample, which is the reason why using intermediate stiffeners throughout link beam to delay shear buckling is suggested by Popov et al. in order to prevent the reduction of link beam capacities and to ensure the stable cyclic response [5]. Popov et al., considering the relationships related to the stability of the shell and plate provided by Timoshenko and Gere [6] (Eq. (1)), provided the Eq. (3) for determining the distance of transverse stiffeners in the I-shaped link beam in terms of the target rotation in the link beam.

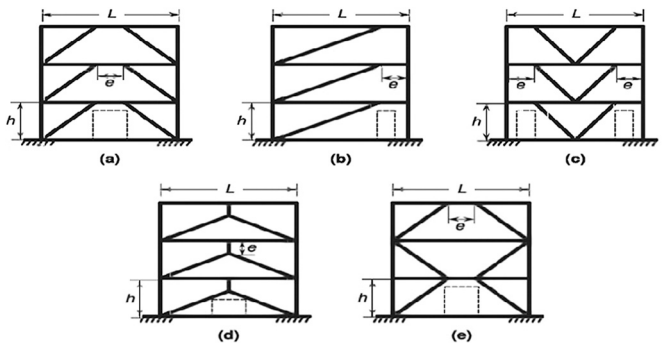

Fig. 1. Common types of eccentrically braced frame [4].

$$\tau_{cr} = k(\alpha)\frac{\pi^2 D}{tb^2} \tag{1}$$

$$D = \frac{Et^3}{12(1-\vartheta^2)} \tag{2}$$

$$\gamma_u = 8.7k(\alpha)\left(\frac{1}{\beta}\right)^2 \tag{3}$$

The use of stiffeners in the link beam makes the design more expensive and also reduces the speed of execution. In addition, the use of stiffeners causes stress concentration in the vicinity of the stiffener weld to the beam's web as well as the creation of residual stress and weaker steel in the area around the weld, caused by welding operations in the link beam. According to Okazaki et al. [7] as well as Ming Lian et al. [8], most fractures in the link beam with intermediate stiffeners, start from the mentioned location (Fig. 2) and then continue in the entire depth of the beam in the vicinity of the stiffener, thus, one of the advantages of removing transverse stiffeners in the beam is the uniformity of the

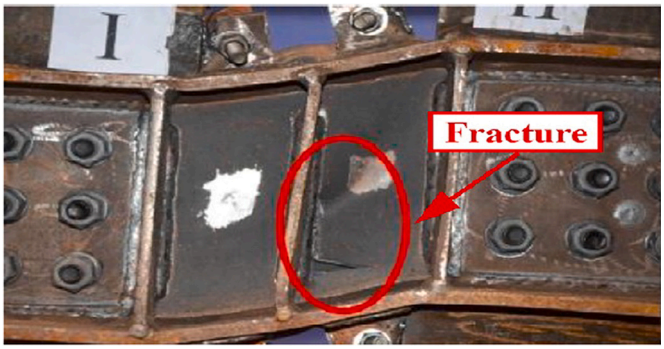

Fig. 2. Fracture in the link beam with intermediate stiffener [8].

distribution of stress and strain in the cross-section and thus the lack of concentration of stress in the vicinity of stiffeners [9].

1.1. Box link beam

In eccentrically braced frames, two types of I-shaped and box link beam are common. In places where it is not possible to insert a lateral brace at the end of the link beam (between the core of the two elevators or in cases where the façade does not allow lateral braces or some bridges), the use of a box link beam, due to high torsional stiffness (if the moment of inertia about the weak axis is more than 67% of the moment of inertia about the strong axis), prevents lateral torsional buckling [3]. Bruneau and Berman [10,11] in the United States conducted a lot of theoretical and experimental research on the behavior of box link beams as one of the most suitable methods for retrofitting bridges. According to Bruneau and Berman's researches, using hollow structural sections (HSS) as a link beam in eccentrically braced frame, the maximum link beam length is obtained equal to 460 mm in order to ensure shear behavior, which is due to the shortness of this length relative to the span length in common structures, in the lateral interstorey drift ratio about 0.5%, the plastic rotation of the link beam exceeds 0.08 rads and this type of link beams do not show proper behavior in the structure and the use of HSS in the link beam is not recommended.

Flange buckling in the link beam is known as an inappropriate limit state, because following the flange buckling in the link beam, lateral torsional buckling occurs and, in turn, may result in severe degradation of strength and reduced ductility. According to studies of Bruneau and Berman [10], flange buckling occurs in box link beam when the average axial stresses caused by bending moment at the end of the link beam reaches 1.29 times the yield stress of the flange material, and in order to avoid the occurrence of flange buckling, the maximum compactness ratio of flange in the box link beam with shear behavior is theoretically obtained from the Eq. (4) [10].

$$\frac{b_f'}{t_f} \le 1.00\sqrt{\frac{E}{F_{yf}}} \tag{4}$$

Bruneau and Berman [11] similar to Popov et al.'s [5] studies on I-shaped link beams, determined the maximum distance between the intermediate stiffeners in the box link beam in order to prevent shear buckling in the web and to ensure stable hysteresis behavior, according to the maximum demand of the expected plastic rotation in the link beam as Eqs. (5) and (6) for two conditions with a stiffener distance less or greater than the depth of beam [10].

$$\frac{a}{t_w} + \frac{1}{8}\frac{d}{t_w} = C_B \quad a \le d \tag{5}$$

$$\frac{a}{d} = \sqrt{\frac{5.34}{\left(\frac{\gamma_u \left(\frac{d}{t_w}\right)^2}{4.35}\right)} - 4} \quad a > d \tag{6}$$

C_B is determined according to the amount of inelastic limit rotation in the link beam and for rotations 0.08 and 0.02 rads are considered to be 20 and 37, respectively.

The minimum cross-section of stiffeners is obtained from the Eq. (7) in order to prevent buckling when it forms a tension field in the web of box link beam [10].

$$A_{st} \ge \frac{F_{uw} t_w a}{0.828 F_{yst}} \left(1 - \frac{\frac{a}{d}}{\sqrt{1 + \left(\frac{a}{d}\right)^2}}\right) \tag{7}$$

Bruneau and Berman [11] also using finite element modulation and conducting multiple tests provided the permissible compactness ratios for flanges and webs of box link beams with yield stresses between 250 and 450 MPa, according to Table 1.

According to Table 1, in the link beams with the compactness ratio of the web less than $0.64\sqrt{\frac{E_S}{F_{yw}}}$, there is no need to use the intermediate stiffeners and also with the increase of the compactness ratio of the web than $1.67\sqrt{\frac{E_S}{F_{yw}}}$, the use of the intermediate stiffeners cannot prevent the buckling of the web. In intermediate and long link beams, the mode of failure is often in the form of flange buckling, and consequently the use of intermediate stiffeners has little effect on increasing the buckling capacity of the flange and dissipating energy.

1.2. Link overstrength

Overstrength factor is defined as the ratio of maximum shear force in the hysteresis curve to the amount of plastic shear force in the short link beam or the ratio of the maximum moment at the end of the link to the plastic moment of the section in the intermediate and long link beam. The amount of overstrength factor is often higher for the shear link beams than the bending and intermediate types. Overstrength changes as a function of the compactness ratio of the web in the short link beam and as a function of the flange compactness ratio in the long link beam. As mentioned, in the eccentrically braced frame, the force-controlled components are designed based on the capacity of the link beam; To this end, other components should be designed for the maximum force created in the link beam, taking into account the types of factors that

Table 1
Permissible compactness ratios in box link beams.

Link beam behavior	Compactness ratio	Maximum allowable compactness ratio
Shear	Flange $\frac{b'}{t_f}$	$1.00\sqrt{\frac{E}{F_{yf}}}$
	web $\frac{d'}{t_w}$ (with stiffener)	$1.67\sqrt{\frac{E}{F_{yw}}}$
	web $\frac{d'}{t_w}$ (without stiffener)	$0.64\sqrt{\frac{E}{F_{yw}}}$
Intermediate	flange $\frac{b'}{t_f}$	$0.64\sqrt{\frac{E}{F_{yf}}}$
	web $\frac{d'}{t_w}$	$0.64\sqrt{\frac{E}{F_{yw}}}$
Flexural	flange $\frac{b'}{t_f}$	$0.64\sqrt{\frac{E}{F_{yf}}}$
	web $\frac{d'}{t_w}$	$0.64\sqrt{\frac{E}{F_{yw}}}$

create overstrength in the link beam. Factors that create overstrength are: strain hardening of link beam materials, expected yield stress of the materials to nominal yield stress ratio (coefficient in R_y in AISC seismic provisions), flange participation in shear bearing, and effects caused by composite behavior of beam and slab.

According to experimantal studies, link beam is able to provide a lot of strain hardening. The test shows the value of overstrength in I-shaped link beam for ASTM A992/A992M steel between 1.2 and 1.45; Also, the overstrength coefficient for ASTM A36/A36M is considered to be 1.5. In 2014, Mohebkhah et al. [12], using numerical modeling, conducted studies on the overstrength coefficient of I-shaped shear link beams and found that overstrength factor provided by the U.S. Steel Structures Design codes for link beams is non-conservative and suggested overstrength factor for shear link beams between 1.53 and 1.77. According to Cheng et al. [13] by reducing the normalized length of the link beam, the flange's participation in tolerating of shear forces increases and thus the overstrength factor of the link beam increases.

In large bridges, the value of overstrength factor has been reported up to 2, indicating the effect of the geometry of the link beam on the value of the overstrength factor. Berman et al. [11] showed that the overstrength factor due cyclic strain hardening for box link beam was 11% higher than I-shaped link beam. The maximum expected shear in the link beam (V_{ult}), is calculated from multiplying the amount of plastic shear (V_p) and the cyclic hardening coefficient (Ω), and the ratio of actual yield stress to nominal yield stress (R_y) in accordance with the Eq. (8) [11].

$$V_{ult} = \Omega R_y V_p \tag{8}$$

According to AISC 341–16 [3], the cyclic hardening coefficient for I-shaped link beams is 1.25 and in box link beam is considered to be 1.4.

1.3. Low yield point steel

In general, the steel used in structural components designed to dissipate earthquake energy hysteretically, should have characteristics such as low yield stress, high ductility and high energy dissipation capability, stable hysteresis cycles, suitable low cycle fatigue characteristics, and sufficient elastic stiffnesss for stability against wind and small earthquakes [14]. Reducing the yield point of the steel used in the passive dampers of structures, facilitates the possibility of earlier yielding of the dampers than other force-controlled elements of the frame. Considering the equality of elasticity modulus of low yield point steels and reducing their yield point compared to conventional steels, the problem of non-participation of passive metallic yield dampers in the dissipation of structural energy in small lateral displacements can be reduced, because yield strain in low yield point steels is far less than conventional structural steels. Also, by yielding of the steel dampers in small lateral displacements, the structure becomes softer and its time period increases, which can also reduce the base shear in the structure. In 1986, Japanese researchers began working on the production of steel with the aforementioned specifications, for the sake of using in structural fuses. To this end, by reducing the amount of alloys used in steel, combining nitrogen and carbon using alloys such as titanium, rolling control and steel operation by controlling the temperature after rolling and increasing the size of crystals, low yield point steel, called LYP100, was first manufactured by Japanese company Nippon Steel [14]. After Japan, researches in China also led to the construction of low yield point steel, with nominal yield stresses of 100, 160, and 225 MPa, which were widely used in the design of structural fuses [15].

According to Yamaguchi et al.'s research [16], low yield point steel made in Japan has nominal yield stress between 85 and 120 MPa and ultimate stress of 200 to 300 MPa and its modulus of elasticity is equal to conventional construction steel. The ultiamte strain in this type of steel is more than 50%, which indicates high ductility and the ability to withstand high strains. By changing the thickness of this steel, the yield stress of the samples changes in a small range, and also this steel shows a significant isotropic strain hardening. The ratio of yield stress to ultimate stress in this type of steel is 0.34, which allows proper redistribution of force after its yielding. Also due to the low amount of carbon, this type of steel shows a good weldability.

Gang Shi et al. [15] in 2017 investigated the mechanical properties and constitutive model of low yield point steel made in China under monotonic and cyclic loading and presented the parameters of the strain hardening model for these materials. The ratio of yield stress to ultimate stress for low yield point steel LY100, LY160, and LY225 was 0.51, 0.63, and 0.66, respectively. Gang Shi et al. [17] also observed that the ultimate strain of the mentioned steels was more than 40%, indicating their proper ductility capacity.

Dusicka et al. [18] loaded a large number of different types of steel under cyclic loading and observed that low yield point steel showed considerable strain hardening in cyclic loading. According to this research, the maximum ultimate stress observed for low yield point steel under cyclic loading is 4.8 times its yield stress, which is about 2.5 times more than that for conventional structural steels.

According to Nakashima et al.'s studies [19] on shear panels made of low yield point steel, taking into account considerable strain hardening in low yield point steel, the amount of energy dissipation in this type of steel compared to steel with equal yield stress and elastic perfectly plastic behavior is about 1.5 to 2 times more. Also, using low yield point steel in shear panels, Nakashima et al. observed that the hysteresis behavior of the structure becomes more stable and the shear buckling of the plate is more delayed than conventional steels. The strain hardening of the low yield point steel causes that after yielding, the lateral stiffness of the frame does not drop severely so as to prevent the creation of soft storey in the structure [20].

Li-Yan et al. [21] in 2015 studied the behavior of a shear panel using low yield point steel LYP160 made at BAO Steel company in China and suggested a compactness ratio of shear panel to eliminate stiffeners, between 25 and 35. They observed that strain hardening in the mentioned steel, on the one hand, increases energy dissipation and, on the other hand, causes overstrength up to 3.7 in shear panel.

De Matteis et al. [22] studied the use of low yield point steel shear panels in the moment resisting frame in order to increase its lateral stiffness and damping, and observed the use of low yield point steel shear panels can reduce the interstorey drift by about 50% and reduce damage to the main members in the moment resisting frame, and also by using low yield point steel and removing stiffeners in shear panel, early buckling of shear panel can be prevented.

Chen et al. [23] conducted an experimental and numerical study on steel shear walls with boundary elements made of ordinary structural steel and shear panel made of low yield point steel in order to remove stiffeners. They observed that using low yield point steel with a compactness ratio of less than 80 and removal of stiffeners, the shear wall is able to behave properly to the lateral interstorey drift between 3% and 6%. It is also possible to reduce the incidence of Pinching phenomenon. According to Bahrebar et al.'s studies [24], using steel with yield point of 100 MPa in steel shear wall, the maximum compactness ratio of the wall can be increased by 62% and 86% compared to ASTM-A36 and ASTM-A572 Gr50, respectively, without any stiffeners.

Dusicka et al. [25] conducted experimental studies as well as modeling on I-shaped link beams made of steels of yield stress between 100 and 485 MPa and observed that by using low yield point steel and elimination of intermediate stiffeners in the I-shaped link beam, the stress distribution in the link beam was uniform and stress concentration and damage in the vicinity of the intermediate stiffeners in the link beam is prevented so that the ductility of the I-shaped link beam made of low yield point steel can be increased by about 70%. They also observed that by using low yield point steel in the web of the I-shaped link beam, the overstrength of the link beam reached 4.9.

According to Wang et al. [26], the use of low yield point steel in the core of buckling restrained braces leads to an increase in energy

dissipation and more ductility. They also presented combined strain hardening parameters for LYP100 steel. Chen et al. [27] studied the behavior of concentrically braced frame with buckling restrained brace made of low yield point steel, and observed that the use of low yield point steel in the core of the buckling restrained brace causes yielding in lower strains and, so that the energy dissipation of the braces begin in a lower drift. Due to the considerable strain hardening of low yield point steel, the maximum bracing force up to about 2.44 times its yield force and its ultimate length change is about 24 times the deformation corresponding to the steel core yield.

Al Kajbaf et al. [28] in 2018 studied posttentioned energy absorbing connections. Using low yield point steel at the seat angels, they observed that the interstorey drift corresponding to the fracture of angels increased from 4% to 7%, and the energy dissipation in the connection increased between 38% and 222%.

In 2013, Zirakian et al. [29] studied the buckling behavior of steel plates made of low yield point steel whithout stiffeners. Due to the low yield stress in this type of steel, the permissible maximum compactness ratio for buckling of plate after its yield, for simple and rigid boundary conditions is 58% and 86% more than A572 GR50 steel, respectively. Also, due to the considerable strain hardening of LYP100 steel, the tangent modulus after yielding is higher than conventional steels, which increases the critical stress of non-elastic shear buckling.

2. Modeling of finite elements

In general, there are three general methods for solving the problems in civil engineering, including (a) empirical method, (b) exact solution, and (c) numerical method. The finite element method is known as the numerical method of solving problems and is known as the approximation method for the problems of the continuum, which divides the continuum into a limited number of parts. In this way, the behavior of each part is characterized by a limited number of effective parameters and the differential Equations often determine the relationships between these parameters. The behavior of the whole investigated system is derived from the the assembling of the members of the whole system. Abaqus software is one of the finite element softwares that is used in solving various engineering problems, so that the software can solve problems ranging from simple linear analysis to the most difficult nonlinear problems.

2.1. Verification of modeling accuracy

To evaluate the accuracy of the finite element modeling, a sample of a box link beam without intermediate stiffeners and another sample with intermediate stiffeners tested by Berman et al. [11] were used in order to compare the test results with the results of finite element modeling. The cross-section specifications of the samples as displayed in Fig. 3 are presented in Table 2.

The length characteristics of the samples are also presented in Fig. 4.

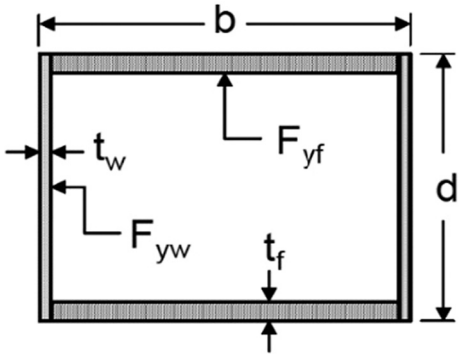

Fig. 3. Geometric parameters of the box link beams.

Table 2
Sample specifications.

Sample	b (mm)	t_f (mm)	d (mm)	t_w (mm)
X2L1.2	209.6	12.7	266.7	6.4
X3L1.2	238.1	22.2	158.8	12.7

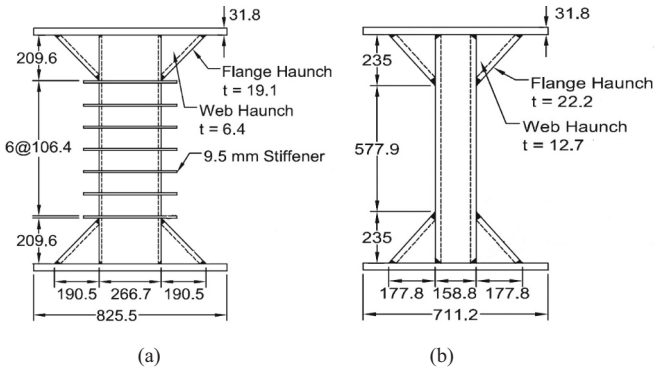

Fig. 4. Specifications of (a) Sample X2L1.2; (b) Sample X3L1.2.

The normalized length of link beams in both samples is considered to be 1.2; The difference between the two samples is the use of intermediate stiffeners, which the X2L1.2 sample has intermediate stiffeners and the X3L1.2 sample lacks it. In the sample with intermediate stiffeners, the width of the intermediate stiffener is 66.7 mm and their thickness is 9.5 mm.

To prevent the residual stress and stress concentration at the end of the flanges, the end stiffeners are not welded to the flanges of the link beam. Also, In order to gradually change the cross-section of the link beam and avoid possible fractures, the haunches are placed at the two ends of the link beam, which due to the strengthening of the link beam in the areas with haunches, yielding and non-elastic behavior is limited to the non-haunched area in the link beam.

In order to model the studied samples, the incompatible solid elements of C3D8I have been used. It should be noted that in solid elements with reduced integration (C3D8R), only degrees of transitional freedom are considered and there is no degree of rotational freedom in the nodes of these elements. So in this study, incompatible solid elements with modified formulations have been used to consider rotational changes in the elements. The meshed form of the samples is presented in Fig. 5.

Considering the fact that existence of geometric imperfection and residual stress due to the process of production, welding, transportation, etc. is unavoidable, in order to increase similarity of modeling to real conditions, it is necessary to consider geometric imperfection in the modeling. In order to determine the size of geometric imperfection, different studies have presented different results, but according to EN-1993-1-5 [30] the size of the initial geometric imperfection is limited to 1/200 of the smallest side of plates. Also, often the shape of geometric imperfection is determined in accordance with the first modes of the

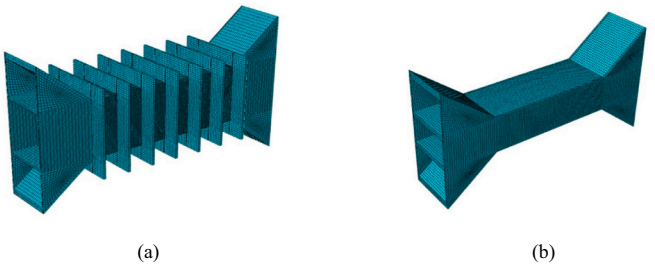

Fig. 5. How to mesh samples; (a) The meshed form of the sample X2L1.2; (b) The meshed form of the sample X3L1.2.

elastic buckling.

In order to analyze the above samples, considering the remarkable non-elastic behavior in the samples and for better convergence during analysis, the method of dynamic implicit in the quasi-static form has been used.

2.1.1. Models boundary conditions and loading

In order to simulate the actual boundary conditions of the link beam in the eccentrically braced frame, the test setup is set in a way to prevent the rotation of the two ends of the link beam; Also, in order to not create axial force in the link beam, the degree of transitional freedom in the axial direction is set free at one end of the link beam. Loading in the samples has been performed as a transitional displacement, perpendicular to the longitudinal axis on the link beam in accordance with the loading protocol provided in AISC 2002 seismic provisions for link beams. The boundary conditions of the samples are displayed in Fig. 6.

The mentioned protocol is presented in terms of the rotation of the link beam, which in order to convert the rotation to vertical displacement at the end of the link beam, the values of the rotation mentioned in the loading protocol should be multiplied by the length of the link beam. The intended loading protocol is displayed in Fig. 7.

2.1.2. Material specifications

In the seismic design of the structures, it is expected that the ductile members in the structures will be able to withstand the big cyclic non-elastic deflections for the purpose of energy dissipation in the severe earthquakes; Therefore, proper modeling of the non-elastic behavior of structural fuses when using finite element softwares is of particular importance. In general, time independent plasticity is subject to three factors: yield criterion, flow rule, and strain hardening rule of materials. In general, the steel used in the structures is subjected to multi-axial stress conditions, therefore, there is a need for criterias for determining steel yield under different stress conditions. One of the most widely used yield criteria in steel is von-Mises yield criterion. Von-Mises stated that the yield criterion in metals were independent of the hydrostatic stresses inflicted on them and presented his yield criterion based on the second invariant of the deviatoric stress tensor. Von-Mises finally, by defining the equivalent von-Mises stress for isotropic materials in accordance with the Eq. (9), stated that when this stress reaches the stress of uniaxial yielding of the material, yielding occurs.

$$\sigma_e = \frac{1}{\sqrt{2}}\left[(\sigma_x-\sigma_y)^2+(\sigma_y-\sigma_z)^2+(\sigma_z-\sigma_x)^2+6\left(\tau_{xy}^2+\tau_{xz}^2+\tau_{zy}^2\right)\right]^{\frac{1}{2}} \quad (9)$$

In the above Equation, σ represents the axial stresses and τ represents shear stresses of the intended element.

After satisfying the yield criterion in the elements of the material, the intended element is yielded and the plastics strains in the intended element are increased. Flow rule is used to determine the ratios of plastic strain tensor components in elements.

Strain hardening determines how to change the yield surface after the primary yielding. According to the studies, in order to model strain hardening in steel, depending on the type of loading, three types of isotropic, kinematic, and combined hardenings are common. In isotropic hardening, after reaching the initial yielding, the size of the yield surface is enlarged in all directions equally; While in kinematic hardening, the size of yield surface is constant and the yield surface is moved as a rigid surface. In combined hardening, a combination of the two mentioned behaviors does exist. The use of Isotropic hardening alone is not appropriate due to the inability of Bauschinger effect modeling in cyclic loading. In this study, combined hardening model was used to model the strain hardening of steel.

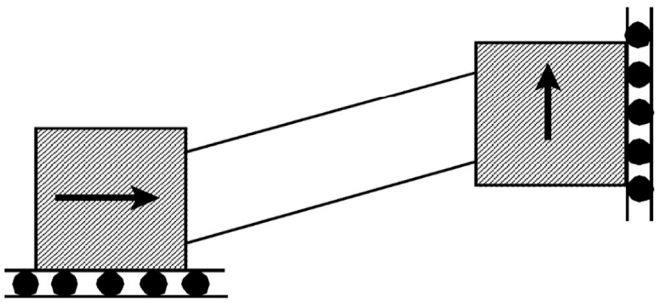

Fig. 6. Boundary conditions of the verification samples.

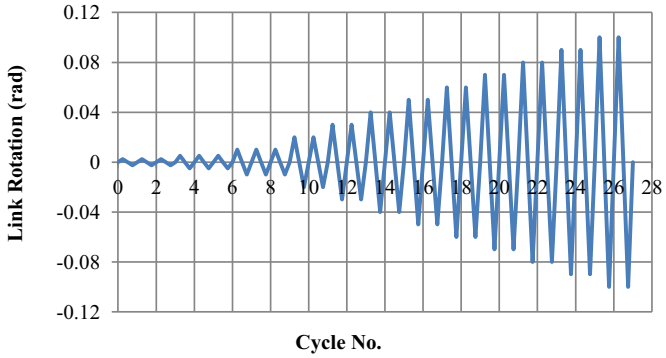

Fig. 7. Loading protocol used for verification.

For all kinds of strain hardening, numerous models are presented. Prager presented the linear kinematic hardening for use in cyclic loadings [31]. Prager's strain hardening is capable of modeling Bauschinger effect, but by using this model, the transition behavior from elastic to the plastic zone is not properly modeled. For the purposes of the deficiencies in the linear strain hardening of Prager, Armstrong and Frederick [32] presented a non-linear kinematic hardening. Finally, Chaboche et al. [33] in order to improve the accuracy of the Armstrong and Frederick model in different intervals of plastic strain, from the interaction of several Equations of Armstrong and Frederick, presented Eqs. (10) and (11) for kinematic hardening.

$$\alpha^k = \frac{C_k}{\gamma_k}\left[1-e^{-\gamma_k \varepsilon^p}\right]+\alpha_0^k e^{-\gamma_k(\varepsilon^p)} \quad (10)$$

$$\alpha = \sum_{k=1}^{n}\alpha^k \quad (11)$$

The amount of ${\alpha_0}^k$ is equal to 0 and $-\frac{C_K}{\gamma_k}\left(\frac{1-e^{-\gamma_k \Delta \varepsilon^p}}{1+e^{-\gamma_k \Delta \varepsilon^p}}\right)$ for monotonic and cyclic loadings respectively. In order to model hardening with appropriate accuracy, the use of at least 2 backstresses has been suggested by researchers. Also, Chaboche et al. [33] presented the size of the yield surface similar to Voce studies [34], using Eq. (12) in order to provide combined hardening.

$$\sigma^0 = \sigma|_0 + \sigma_\infty^0\left(1-e^{-b\varepsilon_{eq}^p}\right) \quad (12)$$

In above Equation, b is a constant of the materials.

2.1.2.1. Calibration of chaboche's combined hardening parameters. In order to use Chaboche's hardening model, it is necessary to introduce the C_k, γ_k, σ_∞^0, *and* b parameters which can be determined from the uniaxial cyclic and monotonic tests on the materials under investigation. In the first step, the σ_∞^0 and b parameters (related to the Isotropic hardening) should be determined (parameter $\sigma|_0$ shows the stress corresponding to zero equivalent plastic strain in constant strain cyclic test, and its value can be considered equal to the proportional limit of steel in the tensile test). To this end, the uniaxial cyclic test with constant strain is required (Fig. 8). It is worth noting that the steel used in the sample X2L1.2 flange is similar to the steel used in link beam of X3L1.2 sample.

After determining the isotropic strain hardening parameters, the

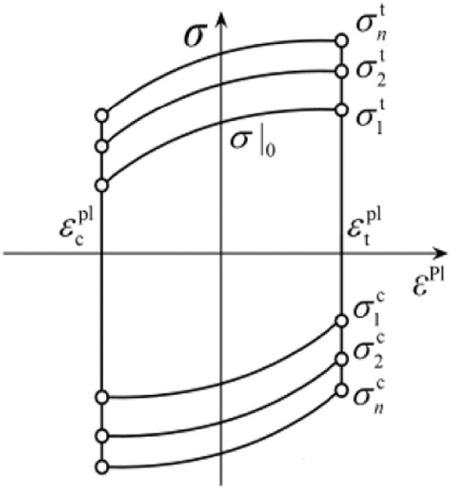

Fig. 8. Constant strain cyclic test.

kinematic hardening parameters should be determined. To this end, both monotonic and cyclic testes were used. The cyclic test with constant strain is used to determine the kinematic hardening parameters in the small plastic strains range and the monotonic test is used to determine the parameters in the larger plastic strains. True strain-stress diagram of the materials used in the samples is shown in Fig. 9.

To calculate the kinematic hardening from the constant strain cyclic test, stabilized cycle should first be determined. A stabilized cycle is a cycle that after that, the shape of strain-stress curve doesn't change (Fig. 10). In fact, in the stabilized cycle, the isotropic hardening value is saturated and its value is constant, and for the same reason in this cycle, hardening is only caused by kinematic hardening.

The values of C_k and γ_k can be determined by trial and error using the least square method. at last, The values of the obtained parameters in Chaboche's combined hardening are listed in Table 3.

The results of finite element modeling and experimentation are shown in Fig. 11.

3. Elimination of the intermediate stiffeners in the box link beam

Limitation of the compactness ratios of webs and flanges in the box link beam and also the overstrength factor provided by Berman and

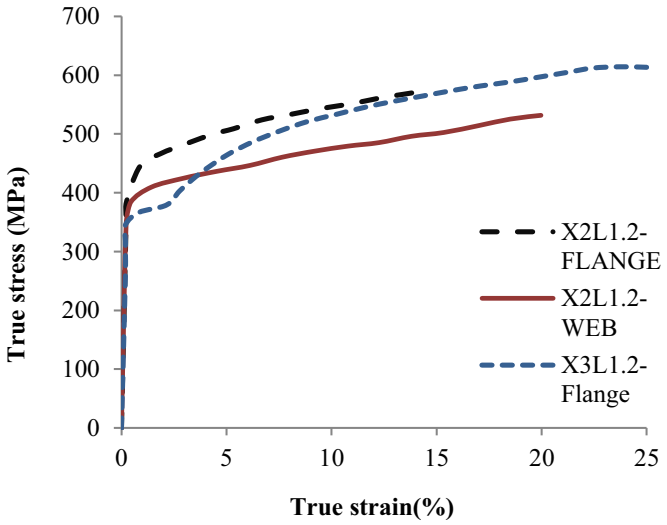

Fig. 9. True stess-strain diagram of the materials used in link beam.

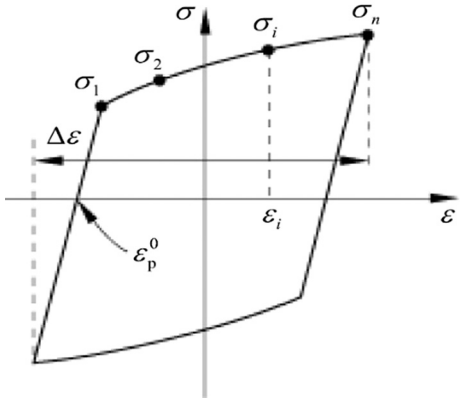

Fig. 10. Stabilized curve chart.

Table 3
Combined hardening parameters of web and flange.

	X2L1.2 Sample web	X2L1.2 Sample Flange	X3L1.2 Sample Flange
C_1 (*MPa*)	42,900	29,100	15,680
C_2 (*MPa*)	4500	1596	1400
C_3 (*MPa*)	680	187	846
γ_1	600	300	280
γ_2	90	13.3	35
γ_3	2	1.7	4.7
$\sigma\|_0$ (*MPa*)	345	345	345
σ_∞^0 (*MPa*)	22	50	81.7
b	5.4	2	2.3

Bruneau [11], are determined for steels with yield stresses of 250 to 450 MPa, so it is needed to review the limitation of the compactness ratio and overstrength factor for box link beam with low yield point steels. In this study, two types of low yield point steel made in Japan and China whose mechanical properties are available in the literature, have been modeled as web of box link beam. In the design of eccentrically braced frame in accordance with the codes of structural design such as U.S. steel codes and Eurocode, shear link beam should be designed against Design Based Earthquake and earthquakes smaller than that as elastic in accordance with the Eq. (13). So, assuming the earthquake demand is equal in the verified link beam with the yield stress of 345 MPa and two types of steel with yield stresses of 85 and 128 MPa, in order to create the equal elastic capacity against the Design Based Earthquake, the thickness of web with low yield point steels should be 4.06 and 2.69 times more than steel with yield stress of 345 MPa, respectively.

$$V_u \leq \varnothing V_n, V_n = 0.6 \cdot A_w \cdot F_{yw} \tag{13}$$

In the design using the above method, attention is not paid to the plastic behavior and due to the significant cyclic hardening in low yield point steel, the amount of overstrength factor in this type of steel is more compared to the values mentioned in the AISC 341–16 for more conventional steels, which can lead to more forces and also non-elastic behavior in braces, out-side-link beams, columns, and connections. Considering the difference in overstrength factor of link beam made of low yield point steel in the web, the net web area of the samples has been determined in such a way that the maximum shear force generated under cyclic loading in the link beam equals the validated sample with intermediate stiffeners. According to preliminary studies, the net area of the beams when using J-LYP100 and C-LYP100 steels should be considered about 4528.72 and 4850.87 mm^2, respectively. The length of all studied link beams is similar to the X2L1.2 sample equal to 648 mm and the behavior of all of them is shear yielding.

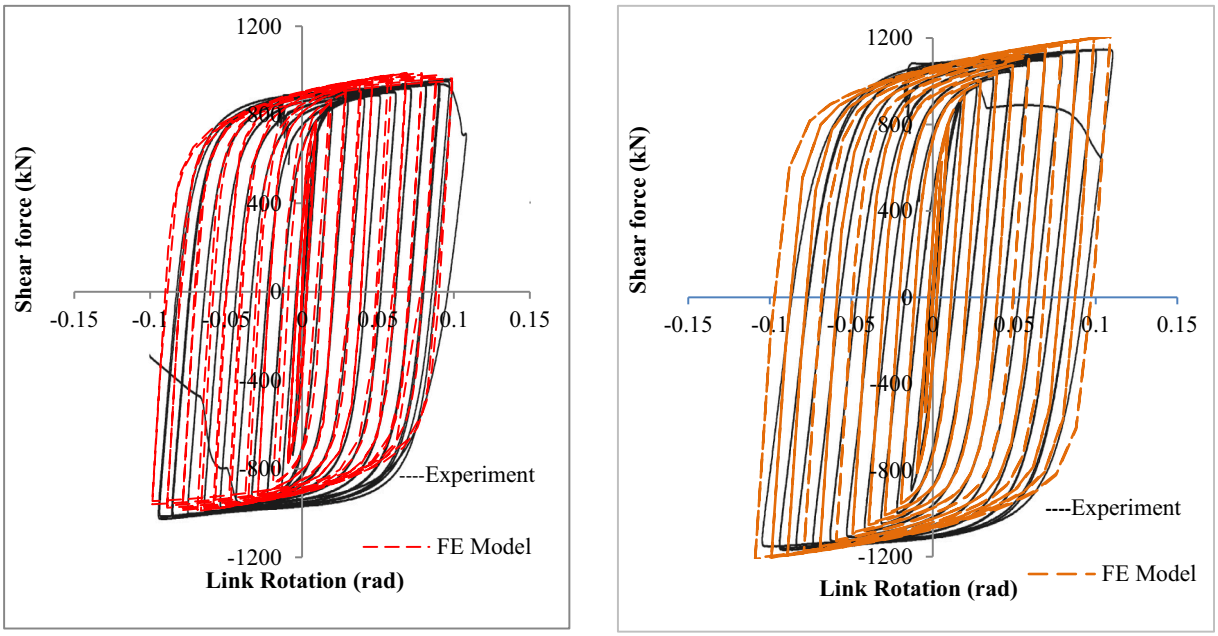

Fig. 11. Comparison of experimental and modeled hysteresis curves; (a) Hysteresis diagram of modeling and test of X2L1.2 sample; (b) Hysteresis diagram of modeling and test of X3L1.2 sample.

3.1. Investigation of different specifications of box link beam made with two types of low yield point steel

In this study, in order to better compare the responses of box link beams made of low yield point steel in web with X2L1.2 sample, in all modeling, mechanical properties of flange steel were selected similar to X2L1.2 sample flanges. For the steel used in web of box link beam, two types of low yield point steel, one low yield point steel made in Japanese company Nippon Steel and the other low yield point steel made in Chinese company Bao Steel, have been used. In order to observe the abbreviation in naming samples, from now on low yield point steel made in Japan is characterized as J-LYP and steel made in China as C-LYP. The mechanical properties of the steels used in the link beam samples are listed in Table 4.

According to AISC 341–16 in link beams with shear yielding behavior, the web and flange of link beam should be seismic compact with high ductility and seismic compact with moderate ductility, respectively. Berman and Bruneau [11] modeled link beams with finite element by changing the compactness ratio of flanges and webs with steels of yield stress between 250 and 450 MPa in order to investigate the maximum permissible compactness ratio in the flanges and webs of link beam. In this research, different characteristics of box link beam have been investigated by changing the compactness ratio of flanges and webs. The maximum compactness ratio of web in link beam without stiffeners is limited to 0.64 $\sqrt{E/F_{yw}}$ according to Berman and Bruneau researches. The investigated compactness ratios of box link beam with low yield point steel are shown in Table 5.

According to Berman and Bruneau's [11] studies on flange buckling in box link beams, it was observed that if the axial stresses caused by the bending moment at the end of the link beam flanges exceeds 1.29 times of the flange material yield stress, the occurrence of flange buckling at the end of the link beam is likely. Also, in order to prevent the destruction of the flanges of the link beam caused by fatigue when entering the cyclic loads and large strains that form during these cycles, the design codes limit the end moments of the link beams to 1.2 times the plastic moment of the cross section. Considering the mentioned limitations for the moment value at the end of the link beam, the dimensions of the flanges in the modeled samples are conservatively adjusted in such a way that the amount of moment created in the flanges at the end of the link beam is limited to 1.2 times of the plastic flange moment according to the Eq. (15) (the stress created in the materials at the end of the flange is less than 1.2 times the yield stress of the materials).

Table 4
Elastic and plastic properties of steels used in modeling.

Steel Type	A572 Gr.50	J-LYP100	C-LYP100
Modulus of elasticity (GPa)	200	200	200
Poisson's ratio	0.3	0.3	0.3
Density ($\frac{Kg}{m^3}$)	7850	7850	7850
Yield Stress (MPa)	345	85	128
σ^0_∞ (MPa)	50	198	145
b	2	5	6
C_1 (MPa)	29,100	32,123	2850
γ_1	300	850	300
C_2 (MPa)	1596	630	1260
γ_2	13.3	89	195
C_3 (MPa)	187	128	1670
γ_3	1.7	20	90
C_4 (MPa)	–	482	330
γ_4	–	0.5	2

Table 5
Compactness ratios in modeling.

Flange Compactness Ratio	C-LYP100 Web Compactness ratio	J-LYP100 Web Compactness ratio
8	12	12
12.5	15.4	15.4
17	16	16.5
21	18	18
25	21	21
40	25.3	24
	–	31

$$M_P = M_{Pf} + M_{Pw} \tag{14}$$

$$M_{Pf} = F_{yf} \cdot b_f' \cdot t_f \cdot (d - t_f) \tag{15}$$

$$M_{Pw} = F_{yw} \cdot \frac{t_w \cdot d^2}{2} \tag{16}$$

In order to distinguish between the names of the samples, the beginning of the name of each model, starts with the type of low yield point steel used in the web, then the compactness ratio of the web, and finally the ratio of the flange compactness is added. In order to model the samples in Abaqus software, concerning the small thickness of the plates, 8-nodes and second order S8R5 shell elements have been used.

Richards et al. [35] showed in 2003 that the AISC 2002 seismic provisions loading protocol imposed a 60% more cumulative plastic strain on link beams than the samples studied under seismic loading, which is why the behavior of the link beam may be unrealistic by using the mentioned loading protocol. To modify the AISC 2002 seismic provisions loading protocol, Richards et al. provided a new loading protocol by investigating the link beams' behavior under different earthquakes so that the new loading protocol was added into this codes from the AISC 2005 version. Comparison of the aforementioned loading protocols is presented in Fig. 12.

In the modeling of all samples, in order to consider the initial geometric imperfection in the model, first, the eigenvalue analysishas been performed and the imperfection size is 1/200 times of the smallest net width of the flange and web in the modeling.

3.2. Important parameters in the study of the responses of link beams

Since shear in short link beams is classified as a displacement controlled component, rotational shear capacity in this type of link beam is considered as one of the most important criteria for investigating the response of link beams. The maximum amount of non-elastic rotation in the AISC 341–16 is limited to 0.08 rads in order to prevent the complete destruction of concrete slab above shear link. In Berman and Bruneau's [11] studies, the maximum permissible rotation (0.08 rads) in the link beam is considered as the target rotation in order to determine the limitations of compactness ratios in the link beam. The limit rotational capacity of a link beam is determined as a plastic rotation in which the shear force in the Backbone curve of the hysteresis diagram reaches to 80% of the maximum shear force. In fact, in the above definition, the strength degradation of the link beam is ignored by 20% in calculating the limit rotational capacity of the link beam. The compactness ratio of web in the intended link beam is acceptable if the limit rotational capacity of the link beam is higher than the target rotation (0.08 rads).

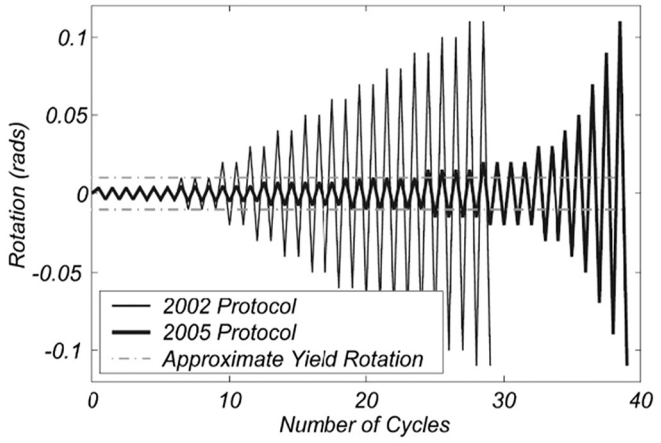

Fig. 12. Comparison of link beam loading protocols in AISC 2002 and AISC 2005 seismic provisions [11].

One of the other important parameters in the behavior of link beams is their overstrength factor. As mentioned above, isotropic strain hardening in low yield point steel is several times more than conventional structural steels, which can significantly increase the overstrength factor in link beams made with low yield point steel. Regardless of the overstrength of low yield point steel link beams, the design of eccentrically braced frame force-controlled elements is done non-conservatively, which can cause damage to these elements and disrupt the response of the structure. According to Berman and Bruneau's studies, in addition of webs, flanges of the link beam also contibute in shear capacity. Therefore, in order to determine the plastic shear capacity of link beam, in addition to the Eq. (13), they also provided three other Equations.

3.2.1. Method 1: Considering box links corners in shear capacity

In this method, in addition to the pure depth of the web, it is assumed that the cross-section corners in the box link beam are also able to withstand the shear, and thus in this method, instead of using the pure depth of the web, the total depth of the beam is used in calculating the plastic shear capacity of the cross-section according to the Eq. (17).

$$V_{p1} = \frac{2}{\sqrt{3}} F_{yw} t_w d \tag{17}$$

3.2.2. Method 2: Considering the share of shear tolerated by flanges

In this method, it is assumed that after the formation of flexural plastic hinges in the flanges, they begin to tolerate some shear. Berman and Brunean presented the plastic shear capacity in the box link beam, taking into account the shear capacity of the beam flanges and assuming the yield stress of flanges equal to that of webs. In this study, considering the difference in steel yield stress in the flanges and webs of the studied samples, the plastic shear capacity of the cross-section is presented with the assumption of different yield stresses in the flanges and webs in accordance with the Eqs. (18) and (19).

$$V_{p2} = V_P + 2V_f \tag{18}$$

$$V_f = \left[1 - \left(\frac{0.49 F_{yw} t_w e}{F_{yf}(b - 2t_w)t_f + F_{yw} t_w t_f}\right)^2\right] \times \left(\frac{F_{yf}(b - 2t_w)t_f^2}{2e} + \frac{F_{yw} t_w t_f^2}{\mathrm{e}}\right) \tag{19}$$

3.2.3. Method 3: Using the shear strength equation of the panel zone

In this method, the shear capacity of the box link beam is determined similar to the shear capacity of the panel zone in the moment resisting frame according to the Eq. (20).

$$V_{p3=} 1.1 F_{yw} d t_w \left(1 + \frac{1.725 b t_f^2}{e d t_w}\right) \tag{20}$$

In this research, the amount of cyclic hardening coefficient is presented by calculating the ratio of maximum shear force to the plastic shear capacity of the box link beam by using the above four methods.

In Eurocode, unlike AISC seismic provisions, the bending capacity of the web in bearing the imposed moments on the link beam cross-section is excluded. In this research unlike Eurocode, Considering the contribution of web in moment bearing capacity of the cross-section in box link beams made of low yield point steel in the web, the flexural overstrength of the web can also be investigated. Although the yield stress of flange is greater than the yield stress of web made of low yield point steel, but the modulus of elasticity of two types of steel is equal; therefore, when the flanges reach the yield strain, the axial strain in the highest fibers of the web is almost equal to the yield strain of the flange, which is also several times the yield strain of the low yield point steel. So, due to the considerable strain hardening of low yield point steel, stress up to several times the yield stress of web are created in it (Fig. 13). For this reason, the ratio of the maximum moment generated in the web at the end of the link beam to the web plastic moment (Eq. (15)) is one of the parameters investigated in the box link beam.

It is worth noting that due to the interaction between the shear and bending, the moment at the end of the web cannot exceed a certain amount.

One of the other effective parameters in the performance of link beams is their energy dissipation. More energy dissipation in the structure increases damping and decreases the structural response. In this study, the amount of energy dissipation by link beams up to the 0.08 rads compared to the energy dissipation of X2L1.2 sample was investigated. If the rotational capacity of the sample is less than 0.08 rads, the energy dissipation of the sample is presented up to its rotational capacity.

In general, in addition to appropriate energy dissipation, link beams must have a good elastic stiffness to reduce the structural response before yield occurs in it. The effective stiffness of link beams in FEMA-356 code [36] is obtained from the combination of shear and bending stiffness according to the Eq. (21).

$$K_e = \frac{K_s K_b}{K_s + K_b} \tag{21}$$

The bending and shear stiffness of the link beam is obtained from Eqs. (22) and (23).

$$K_b = \frac{12EI_b}{e^3} \tag{22}$$

$$K_s = \frac{GA_w}{e} \tag{23}$$

3.3. Results

Different specifications of box link beams with low yield point steels J-LYP100 and C-LYP100 modeled in Abaqus software are presented in Tables 6 and 7.

Considering the rotational capacity values of the modeled samples, it can be observed that by decreasing the compactness ratio of the web, the rotational capacity of the samples generally increases. Flange compactness ratio does not have a completely specific trend with rotational capacity of samples, but it can be stated that in general, by decreasing the flange compactness ratio, the rotational capacity of the samples increases. The rotational capacity of modeled samples is presented by changing the compactness ratios of webs and flanges in Fig. 14. It is worth noting that the rotational capacities presented in some samples due to lack of fracture modeling is calculated to be more than 0.2 rads.

According to the presented results, the maximum permissible compactness ratio of web in box link beams made of low yield point steels made in Japan and China, in order to be of acceptable rotational capacity of link beam without intermediate stiffener is 24 and 21, respectively which is equivalent to $0.5\sqrt{\frac{E}{f_{yw}}}$ and $0.53\sqrt{\frac{E}{f_{yw}}}$ (If the flange compactness ratio is equal or less than 25). Also, the maximum compactness ratio of the web for the mentioned steels was obtained for 16.5 and 16 to prevent any stiffness and strength degradation up to 0.08 rads, respectively (With flange compactness ratio equal or less than 25). It is worth noting that due to the removal of intermediate stiffeners in the box link beam and due to the low flexural stiffness of the flanges, after shear buckling of the web plates, the tension field causes the formation of plastic hinges in the flange of the link beam (with a flange compactness ratio of less than 25) and thus it is not possible to create a full tention field action and the link beam mechanism is done through the creation of the shear plastic hinge. In samples with a flange compactness ratio greater than 25, flange buckling determines the ultimate state of the cross-section (Fig. 15) so the maximum flange compactness ratio in the box link beam is suggested in accordance with the theoretical Equations provided by Berman and Bruneau [10] equal to $\sqrt{\frac{E}{F_{yf}}}$.

According to the results obtained in models with suitable compactness ratio of web, the link beam energy dissipation up to 0.08 rads is larger than the energy dissipation of the sample having intermediate stiffeners and with conventional steel in the web (sample X2L1.2). In general, by increasing the compactness ratios of flanges and webs of the link beam, the energy dissipation of the samples decreases up to 0.08 rads, but the effect of changing the compactness ratio of the web on the energy dissipation of the samples is more significant. Change of the energy dissipation of the studied samples by changing the compactness ratio of flanges and webs is shown in Fig. 16.

In the fourth column of Tables 6 and 7, the ratio of elastic stiffness in samples modeled with low yield point steel to sample X2L1.2 is presented. As can be seen, due to the increase in net web area compared to the reference sample in accordance with the Eq. (23), elastic stiffness has increased in all samples. By increasing the elastic stiffness, the deformation of the structure decreases before the link beam yields compared to the sample made of ordinary steel (assuming the equal lateral force caused by earthquake), but increasing the elastic stiffness of the frame can also increase the absorption of the structural force, which should be examined in the design. In general, by increasing the compactness ratio of the web and decreasing the flange compactness ratio, the elastic stiffness of the link beam increases.

As mentioned above, considerable strain hardening in low yield point steels, on the one hand, leads to increased energy dissipation and, on the other hand, increases overstrength factor in structural fuses. Overstrength caused by cyclic hardening in box link beam with low yield point steel in web, in accordance with the four methods proposed in Berman and Bruneau's research [11] in order to calculate the plastic shear capacity of the cross-section are presented in Tables 6 and 7.

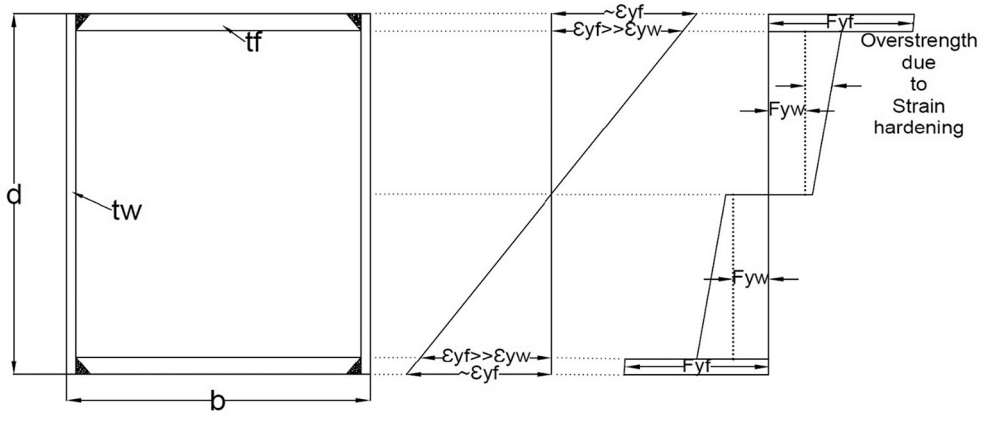

Fig. 13. Axial strain and stress distribution caused by pure bending moment at the end of the box link beam.

Table 6
Effective parameters in the responses of link beam made of J-LYP100 steel.

Sample Name	γ_{up}	Relative energy dissipation	Relative stiffness	Ω_1 Eq. (13)	Ω_2 Eq. (17)	Ω_3 Eq. (18)	Ω_4 Eq. (20)	Ω_{MW} Eq. (16)
J-LYP-12-8	0.235	1.27	1.2	4.65	3.7	3.72	3.72	3.83
J-LYP-12-12.5	0.24	1.23	1.13	4.5	3.72	3.79	3.79	3.4
J-LYP-12-17	0.23	1.19	1.07	4.41	3.73	3.83	3.83	3.12
J-LYP-12-21	0.21	1.15	1.04	4.34	3.73	3.85	3.85	2.84
J-LYP-12-25	0.19	1.14	1.01	4.28	3.72	3.85	3.85	2.73
J-LYP-12-40	0.135	1.02	0.93	4.04	3.61	3.77	3.77	2.35
J-LYP-15.4-8	0.152	1.29	1.26	4.53	3.73	3.8	3.8	3.02
J-LYP-15.4-12.5	0.155	1.25	1.19	4.41	3.75	3.86	3.86	2.63
J-LYP-15.4-17	0.163	1.23	1.16	4.36	3.78	3.91	3.91	2.46
J-LYP-15.4-21	0.143	1.21	1.12	4.26	3.75	3.9	3.9	2.23
J-LYP-15.4-25	0.139	1.18	1.09	4.2	3.73	3.89	3.89	2.22
J-LYP-15.4-40	0.131	1.07	1.02	4.02	3.65	3.85	3.85	2.01
J-LYP-16.5-8	0.129	1.27	1.28	4.39	3.64	3.7	3.7	2.67
J-LYP-16.5-12.5	0.132	1.23	1.21	4.26	3.66	3.77	3.77	2.33
J-LYP-16.5-17	0.129	1.21	1.17	4.19	3.66	3.8	3.8	2.14
J-LYP-16.5-21	0.137	1.2	1.14	4.2	3.72	3.88	3.88	2.08
J-LYP-16.5-25	0.12	1.16	1.11	4.1	3.66	3.83	3.83	1.95
J-LYP-16.5-40	0.111	1.11	1.07	4	3.63	3.8	3.8	1.94
J-LYP-18-8	0.114	1.28	1.3	4.32	3.63	3.72	3.72	2.55
J-LYP-18-12.5	0.121	1.26	1.23	4.23	3.66	3.79	3.79	2.19
J-LYP-18-17	0.124	1.24	1.2	4.22	3.72	3.88	3.88	2
J-LYP-18-21	0.111	1.2	1.16	4.09	3.65	3.82	3.82	1.89
J-LYP-18-25	0.109	1.18	1.14	4.04	3.63	3.81	3.81	1.84
J-LYP-18-40	0.111	1.1	1.07	3.94	3.62	3.82	3.82	1.68
J-LYP-21-8	0.087	1.19	1.34	4.05	3.46	3.57	3.57	2.21
J-LYP-21-12.5	0.096	1.2	1.28	4	3.52	3.66	3.66	1.89
J-LYP-21-17	0.098	1.2	1.24	4.02	3.59	3.76	3.76	1.68
J-LYP-21-21	0.089	1.15	1.21	3.89	3.51	3.69	3.69	1.63
J-LYP-21-25	0.086	1.12	1.19	3.85	3.5	3.68	3.68	1.54
J-LYP-21-40	0.086	1.07	1.12	3.79	3.51	3.72	3.72	1.45
J-LYP-24-8	0.08	1.02	1.37	3.74	3.24	3.35	3.35	1.49
J-LYP-24-12.5	0.084	1.1	1.32	3.8	3.38	3.53	3.53	1.29
J-LYP-24-17	0.084	1.08	1.28	3.75	3.38	3.55	3.55	1.19
J-LYP-24-21	0.072	0.94	1.25	3.63	3.31	3.49	3.49	1.14
J-LYP-24-25	0.082	1.03	1.23	3.67	3.37	3.56	3.56	1.05
J-LYP-24-40	0.073	0.88	1.17	3.6	3.36	3.57	3.57	1.09
J-LYP-31-8	0.079	0.84	1.43	3.27	2.9	3.03	3.03	1.48
J-LYP-31-12.5	0.059	0.78	1.38	3.29	2.98	3.14	3.14	1.4
J-LYP-31-17	0.059	0.77	1.35	3.24	2.98	3.16	3.16	1.27
J-LYP-31-21	0.06	0.76	1.32	3.2	2.97	3.15	3.15	1.22
J-LYP-31-25	0.066	0.8	1.31	3.23	3.01	3.2	3.2	1.18
J-LYP-31-40	0.07	0.79	1.25	3.1	2.93	3.13	3.13	1.21

according to the values of overstrength factors obtained for box link beams made of low yield point steel, it is observed that these values are much higher than those obtained values provided in different design codes in order to design different members of the eccentrically braced frame on the basis of the link beam capacity. Change of the ratio of the maximum shear force created in the link beam to the shear plastic capacity of the link beam (Eq. (13)) is shown in Fig. 17.

As can be seen, by reducing the compactness ratio of the flange and the web, the amount of overstrength factor of link beam increases, and its value for samples of low yield point steel made in Japan is far more than the low yield point steel made in China. The average values of overstrength factor calculated with Eqs. (13), (17), (18), and (20) for samples with JLYP steel were 4.14, 3.6, 3.74, and 3.74, respectively, and for CLYP steel samples were 2.58, 2.25, 2.44, and 2.34, respectively. According to the AISC 341–16, the force-controlled components of the eccentrically braced frame with the box link beam should be designed for the shear force of the $1.4R_yV_P$, in which the number 1.4 represents overstrength factor caused by the cyclic hardening of materials, R_y is the ratio of the expected yield stress to the nominal yield stress, and V_P *is* the plastic shear capacity of the link. So, designing the dimensions of web with low yield point steel, based solely on its yield stress and with the same response modification factor, can lead to damage and non-elastic behavior in other components of the eccentrically braced frame and disrupting their behavior. To avoid this issue, the dimensions of the web plate made of low yield point steel should be determined in such a way that the maximum force created in the link beam made of ordinary steel, is equal to the maximum force created in the link beam made of low yield point steel. It is worth noting that among the Equations presented for calculating the plastic shear capacity in box link beams, the use of Eq. (17) makes the values of overstrength factor in the link beam independent of the flange compactness ratio as well as the lowest coefficients of variations around the average value, and therefore, the use of this Equation and the average values of overstrength factor presented for this Equation are suggested for design purposes.

According to the above, due to differences in yield strain of flange made of ordinary steel and web made of low yield point steel in the box link beam, as well as considerable strain hardening in low yield point steel, the amount of moment at the end of the web of link beam is greater than the plastic moment of web in accordance with the Eq. (16). The values of the ratio of the maximum moment at the end of the web of link beam to its plastic moment are given in the last column of Tables 6 and 7. In addition, the flexural overstrength of the web is generally increased by decreasing the compactness ratio of the web and flange, and the average value for JLYP and CLYP steels is 2.17 and 1.35, respectively.

3.3.1. Box link beam with low yield point steel maximum normalized length for shear yielding behavior

In determining the normalized length of the link beam in order to shear yielding behavior occur in it, AISC seismic provisions presented the length of the link beam according to the Eq. (24).

Table 7
Effective parameters in the behavior of link beam made of C-LYP100 steel.

Sample Name	γ_{up}	Relative energy dissipation	Relative stiffness	Ω_1	Ω_2	Ω_3	Ω_4	Ω_{MW}
C-LYP-12-8	0.21	1.3	1.3	2.82	2.26	2.58	2.29	2.16
C-LYP-12-12.5	0.226	1.26	1.22	2.74	2.28	2.54	2.34	1.83
C-LYP-12-17	0.199	1.23	1.16	2.68	2.28	2.5	2.35	1.7
C-LYP-12-21	0.191	1.2	1.13	2.64	2.28	2.48	2.36	1.63
C-LYP-12-25	0.19	1.18	1.1	2.61	2.28	2.47	2.37	1.49
C-LYP-12-40	0.131	1.07	1.01	2.5	2.24	2.38	2.35	1.37
C-LYP-15.4-8	0.139	1.32	1.37	2.73	2.27	2.54	2.32	1.7
C-LYP-15.4-12.5	0.142	1.28	1.29	2.66	2.28	2.5	2.36	1.47
C-LYP-15.4-17	0.139	1.25	1.24	2.61	2.28	2.47	2.37	1.33
C-LYP-15.4-21	0.132	1.23	1.21	2.57	2.27	2.44	2.38	1.3
C-LYP-15.4-25	0.128	1.21	1.18	2.54	2.27	2.42	2.38	1.21
C-LYP-15.4-40	0.125	1.12	1.1	2.48	2.26	2.38	2.39	1.15
C-LYP-16-8	0.13	1.32	1.38	2.71	2.26	2.52	2.31	1.6
C-LYP-16-12.5	0.142	1.28	1.31	2.66	2.29	2.51	2.37	1.39
C-LYP-16-17	0.139	1.26	1.26	2.62	2.3	2.48	2.39	1.29
C-LYP-16-21	0.12	1.21	1.22	2.54	2.25	2.42	2.36	1.2
C-LYP-16-25	0.139	1.22	1.2	2.56	2.3	2.45	2.41	1.19
C-LYP-16-40	0.119	1.11	1.11	2.44	2.23	2.35	2.35	1.12
C-LYP-18-8	0.115	1.3	1.41	2.62	2.22	2.45	2.28	1.46
C-LYP-18-12.5	0.12	1.29	1.34	2.57	2.24	2.43	2.33	1.27
C-LYP-18-17	0.117	1.26	1.3	2.56	2.27	2.44	2.37	1.13
C-LYP-18-21	0.106	1.23	1.26	2.5	2.24	2.39	2.35	1.08
C-LYP-18-25	0.101	1.21	1.24	2.47	2.23	2.37	2.35	1.04
C-LYP-18-40	0.102	1.14	1.16	2.43	2.24	2.34	2.37	0.99
C-LYP-21-8	0.083	1.21	1.45	2.51	2.15	2.36	2.23	1.29
C-LYP-21-12.5	0.095	1.25	1.39	2.5	2.21	2.38	2.31	1.1
C-LYP-21-17	0.084	1.17	1.35	2.43	2.18	2.32	2.29	1
C-LYP-21-21	0.081	1.11	1.31	2.4	2.18	2.31	2.3	0.97
C-LYP-21-25	0.086	1.17	1.29	2.41	2.2	2.32	2.33	0.92
C-LYP-21-40	0.08	1.03	1.22	2.35	2.19	2.28	2.32	0.96
C-LYP25–8	0.058	0.86	1.5	2.32	2.03	2.2	2.11	1.16
C-LYP-25-12.5	0.06	0.9	1.44	2.31	2.07	2.22	2.18	0.98
C-LYP-25-17	0.057	0.86	1.4	2.27	2.06	2.18	2.18	0.93
C-LYP-25-21	0.057	0.87	1.38	2.31	2.12	2.23	2.24	0.83
C-LYP-25-25	0.055	0.84	1.36	2.28	2.11	2.21	2.24	0.79
C-LYP-25-40	0.06	0.74	1.16	2.15	2.02	2.1	2.15	0.7

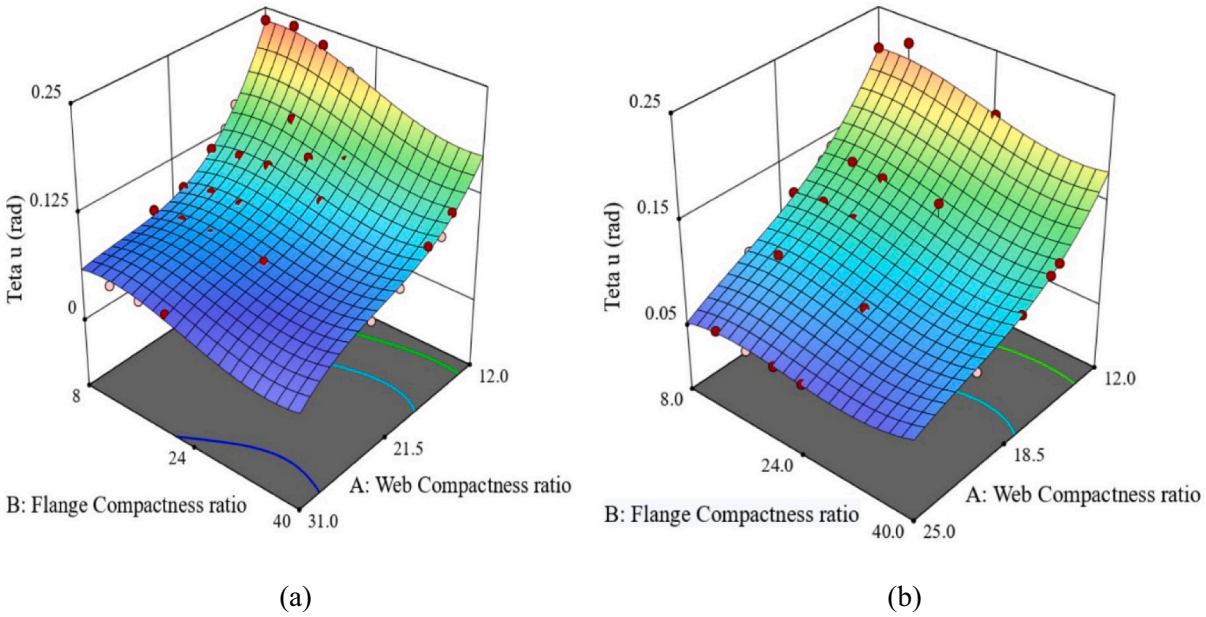

Fig. 14. Change of the rotational capacity of the box link beam by changing the compactness ratios of flanges and webs; (a) The rotational capacity for samples with JLYP steel; (b) The rotational capacity for samples with CLYP steel.

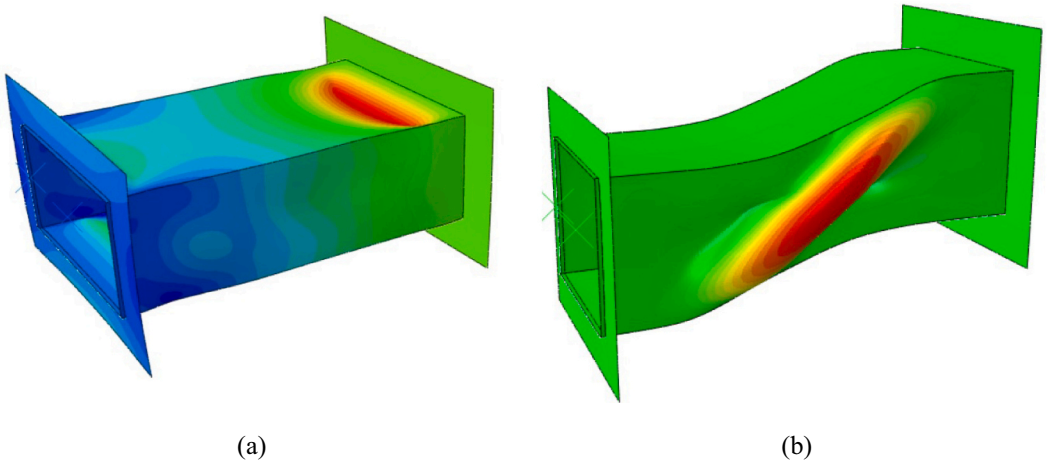

Fig. 15. Ultimate mechanisms of box link beam failure; (a) Buckling of the flange in compactness ratios greater than 25; (b) Formation of plastic hinges in the flange and tension field incompletely.

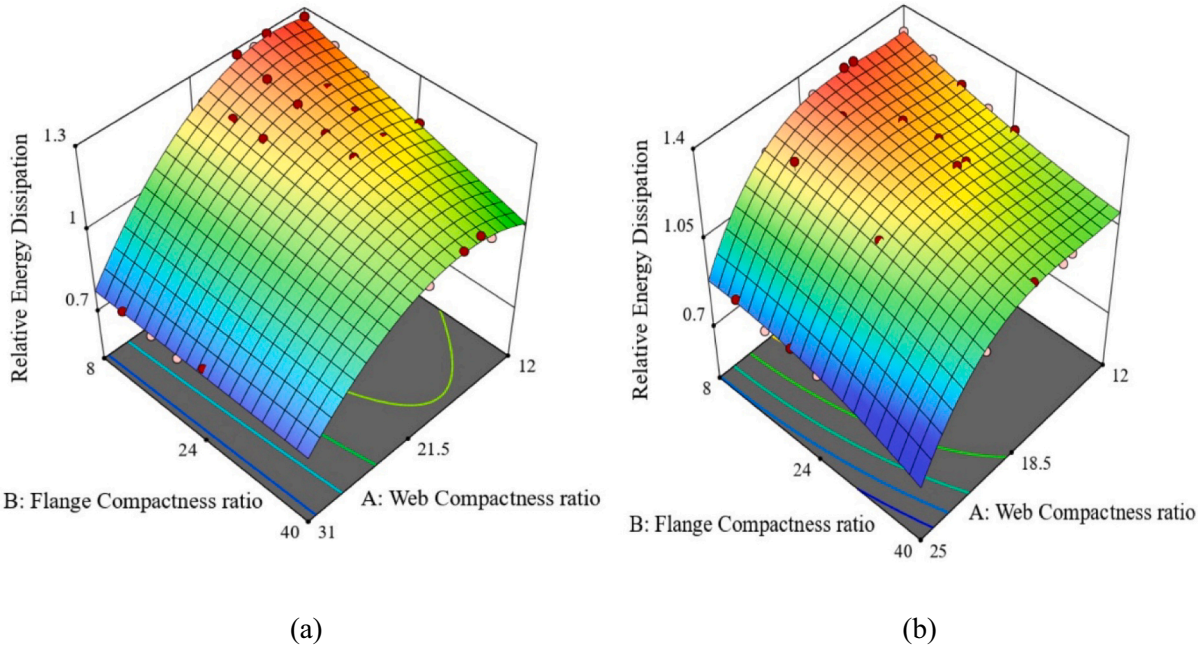

Fig. 16. Change of the relative energy dissipation of the link beam by changing the compactness ratios of flanges and webs; (a) Relative energy dissipation for samples with JLYP steel; (b) Relative energy dissipation for CLYP steel samples.

$$e \leq 1.6\frac{M_P}{V_P} \tag{24}$$

The above Equation is presented with the assumption of overstrength factor of 1.5 times the plastic shear capacity of the cross-section and the moment limiting at the end of the link beam to 1.2 times the plastic moment of the cross-section, but as mentioned above, due to considerable strain hardening in low yield point steel, shear and flexural overstrength of the web in the link beam is greater than the values mentioned in the AISC 341–16, so the minimum amount of plastic moment of the flanges in the box link beam with web made with low yield point steel in order to ensure shear yielding behavior in the link beam is determined in accordance with the Eqs. (25) and (26).

$$M_u = \frac{V_u e}{2} = \frac{\Omega_V V_p e}{2} \tag{25}$$

$$M_u \leq \Omega_M M_{Pw} + 1.2M_{Pf} \tag{26}$$

In the above Equations, V_u is the maximum shear created, taking into account the shear overstrength in the link beam (Ω_V) and M_u is the maximum moment created at the end of the link beam corresponds to the maximum shear force and Ω_M is flexural overstrength of the web of the link beam. According to the above Equations, the minimum plastic moment capacity of flange in the box link beam with web made of low yield point steels J-LYP100 and C-LYP100 is obtained from Eqs. (27) and (28), respectively.

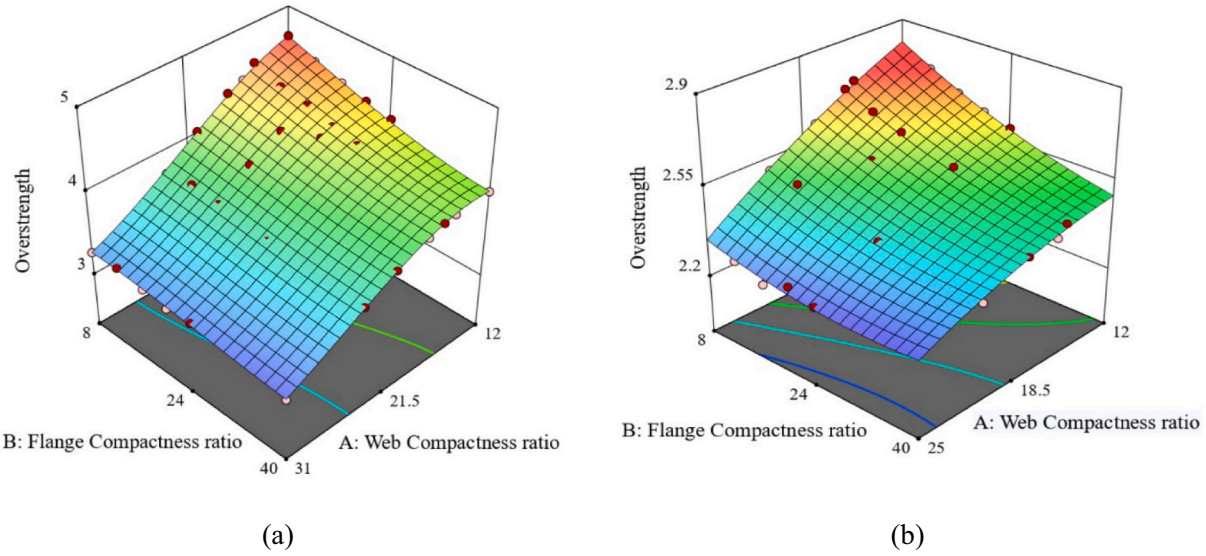

Fig. 17. Change in the overstrength factor of the link beam by changing the compactness ratios of the flanges and webs; (a) Overstrength factor for samples with JLYP stee; (b) Overstrength factor for samples with CLYP steel.

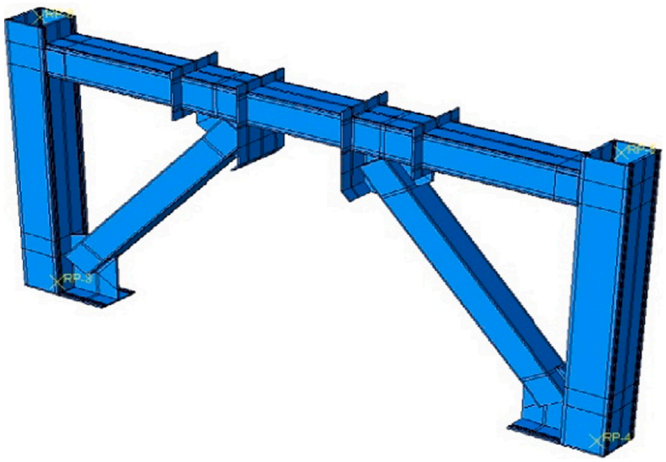

Fig. 18. Designed EBF frame modeled in Abaqus sowfware.

$$M_{Pf} \geq 1.72V_P e - 1.8M_{Pw} \quad (27)$$

$$M_{Pf} \geq 1.07V_P e - 1.12M_{Pw} \quad (28)$$

4. Behavior of eccentrically braced frame with low yield point steel in the web of the link beam

In order to further investigate the behavior of link beam with low yield point steel in eccentrically braced frame, a single storey single span frame as designed in accordance with the design requirements of eccentrically braced frame in AISC 341–16, for the box link beam sample tested by Berman and Bruneau [11] (sample X2L1.2). Considering the values of overstrength factors provided for box link beams with web made of low yield point steel, the dimensions of link beams made with JLYP and CLYP steels are determined so that the maximum shear force of the yielded and strain hardened link beam is equal to the X2L1.2 sample. The compactness ratio of web of link beams made of low yield point steel is 21, and its flange compactness ratio is similar to that of X2LL1.2 equal to 17. In eccentrically braced frame, in order to prevent buckling of gusset plate due to the compressive forces in the box brace, the stiffener is used for the gusset plate, and also unlike the concentrically braced frames, the bracings are as close to the beam as possible. This way, the connection of the brace to the beam in this type of system is done rigidly. In this modeling, a simple connection is used to connect the outside link beam to the column. According to preliminary modeling, if the simple connection is modeled using seat angles or web angles in connecting the beam outside the link to the column, because of the low axial stiffness of these connections and considering that the beam outside the link is under a large axial force, the eccentrically braced frame has not shown appropriate behavior and therefore, the simple connection with shear plates is used. The overall shape and dimensions of the designed frame are presented in Fig. 18 and Table 8. It is worth noting that all frame members are considered box type.

4.1. Investigation of the pushover behavior of eccentrically braced frame

Modeling of the desired frames in Abaqus software was performed using solid C3D8I elements with two elements in the thickness of the webs and flanges of the box link beam. At first, the designed frames have been affected by lateral displacement as a pushover. The target interstorey drift of the frames is determined equal to 2.5%, but the pushover loading has continued up to 1.5 times the target interstorey drift mentioned. It should be noted that according to the modeling, it is clear that due to the flexibility of the frame members, the rotation of the link beam cannot be determined according to the interstorey drift of the floor, as the Equation presented in the AISC 341–16 (Eq. (29)).

$$\gamma_P = \left(\frac{L}{e}\right)\left(\frac{\Delta_i}{h}\right) \quad (29)$$

The change of the rotation of the link beam is compared with the interstorey drift of the frames modeled in Fig. 19.

According to the modeling, it is clear that the lower flange of the link beam in the eccentrically braced frame is more constrained by the end stiffeners of the gusset plate than the upper flange, which is why the corresponding plastic strain at the end of the lower flange of the link beam is higher than the upper flange. The change of the base shear in terms of the interstorey drift of the modeled frames is compared in Fig. 20.

By comparing the diagrams in Fig. 20, it can be observed that by using low yield point steel in the web of the link beam, the web's yield

Table 8
Dimensions of the sections of the designed eccentrically braced frame.

	Frame components	Flange thickness (mm)	Web thickness (mm)	Section height (mm)	Section width (mm)	Section Length (mm)
Specimen with X2L1.2 link beam	Link Beam	12.7	6.4	266.7	209.6	648
	Outside Link Beam	18	6.4	277.3	209.6	1300
	Bracing	10	12	200	160	1898
	Column	20	15	250	265	2012
Specimen with JLYP link beam	Link Beam	12.73	10.89	254.32	238.19	648
	Outside Link Beam	15	10.89	258.86	238.19	1300
	Bracing	10	12	200	160	1898
	Column	20	15	250	280.16	2002
Specimen with CLYP link beam	Link Beam	12.57	11.26	261.58	236.21	648
	Outside Link Beam	12.57	11.26	261.58	236.21	1300
	Bracing	10	12	200	160	1898
	Column	20	15	250	278.20	2004

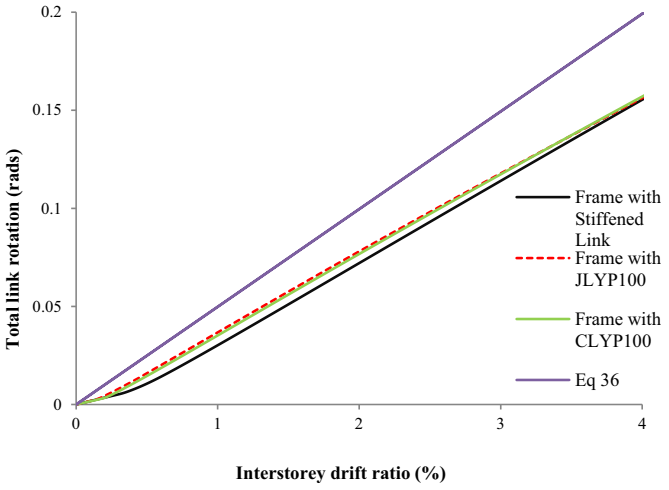

Fig. 19. The change of the rotation of the link beam with the change of the interstorey drift ratio of the floor.

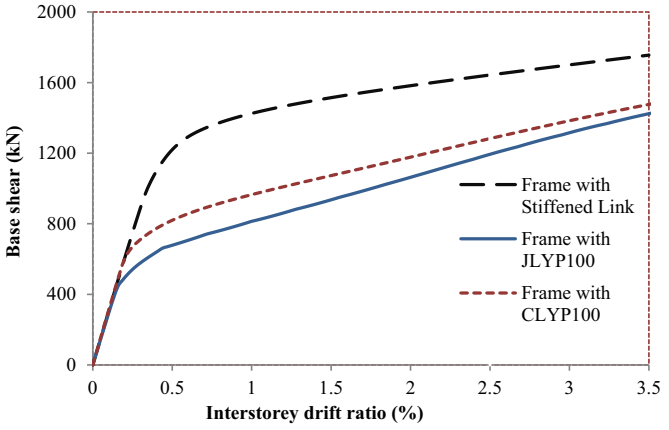

Fig. 20. Pushover curves for different samples of eccentrically braced frame.

happens in the much lower interstorey drift than the frame made of common structural steel. The interstorey drift corresponding to frame yield in link beam with intermediate stiffeners, J-LYP100, and C-LYP100 steel frames equal to 0.31%, 0.13%, and 0.17%, respectively, indicating that the frame with low yield point steel can start dissipating earthquake energy in smaller interstorey drifts, thus increasing the ductility of the structure. Due to the considerable strain hardening in low yield point steel, base shear-interstorey drift diagrams slope after yield of bracing frame with link beam without stiffeners is more than the frame made of link beam with intermediate stiffeners, thus the reserve strength (over-strength) of the frame with low yield point steel is more than the frame with ordinary steel. According to the aforementioned issues and defining the response modification factor of the structure, it is expected that the response modification factor of eccentrically braced frame made of low yield point steel is more than normal eccentrically braced frames.

4.2. *Investigation of cyclic behavior of eccentrically braced frames*

AISC 2005 seismic provisions loading protocol has been used to investigate the behavior of frames modeled under the effect of cyclic loading. This protocol is presented in terms of the rotation of the link beam, so the rotation of the link beam should be converted into interstorey drift. Due to the flexibility of the frame, the existing Equations for converting the rotation of the link beam to the interstorey drift are not of good accuracy, and the interstorey drift value of the frame has been determined by the trial and error method in order to create the specified rotation in the link beam according to the loading protocol. By comparing the hysteresis behavior of the modeled frames, it is clear that in large interstorey drifts, the three studied hysteresis curves almost coincide with each other, indicating equal ultimate lateral bearing capacity in these three frames, but in smaller lateral drifts, it is observed that the lateral forces in the frame with intermediate stiffeners is more than frames made of low yield point steel in the web. so, it is determined that, due to the low yield stress of easy going steels and high strain hardening in these types of steels, the lateral yield force in the frames made of this type of steel is less than the lateral yield force of the frames made of ordinary steels, and the amount of lateral force in the frames with low yield point steel after the yield of the web of the link beam gradually increases with increasing loading until the ultimate lateral capacity of the frame (Fig. 21).

Using low yield point steel link beams, due to the yield of these types of steels in the smaller interstorey drift, energy dissipation starts in

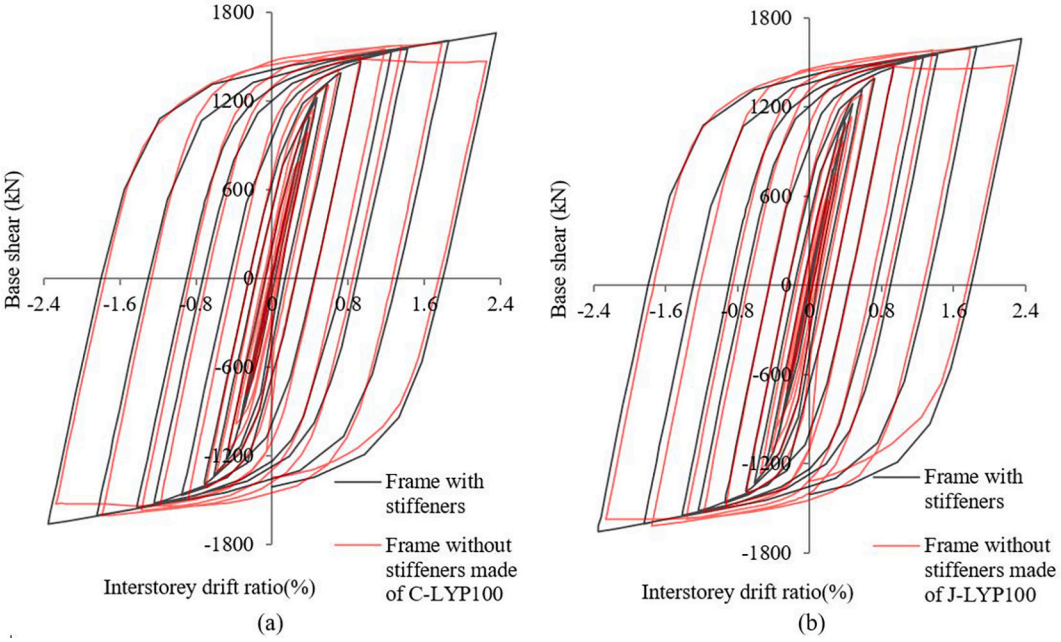

Fig. 21. Comparing hysteresis curves of frame with intermediate stiffeners and frames with low yield point steel; (a) Hysteresis diagram of frame with J-LYP steel; (b) Hysteresis diagram of frame with C-LYP steel.

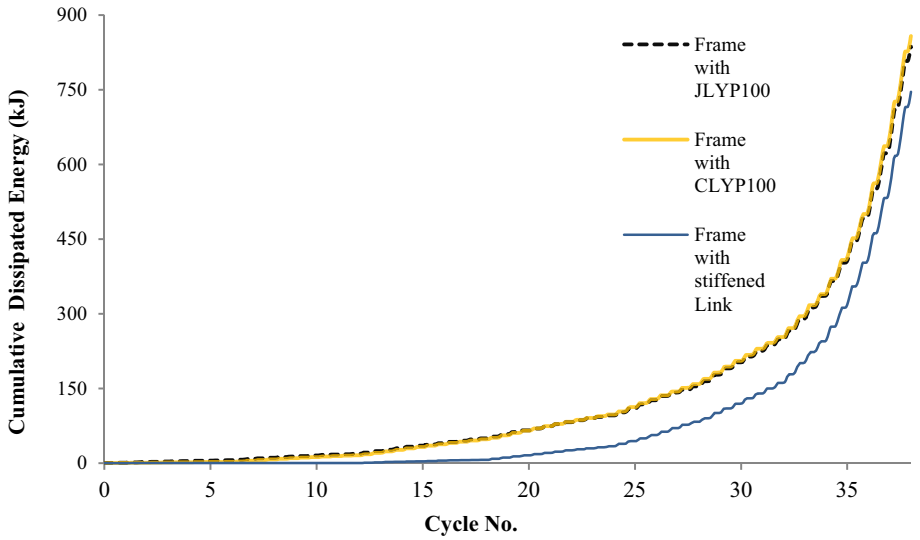

Fig. 22. Comparison of cumulative energy dissipation of modeled frames under cyclic loading.

smaller drifts and the energy dissipation of the link beam gradually increases due to the considerable strain hardening in low yield point steels. The amount of energy dissipation in the frame sample with link beam with intermediate stiffeners, starts later than the samples with soft steel. The capacity of the frame energy dissipation with link beams made of J-LYP100 and C-LYP100 steels, are respectively 1.12 and 1.15 times the capacity of the frame with intermediate stiffeners (Fig. 22).

4.3. Investigation fracture in link beam of eccentrically braced frame

In general, considering that structural fuses may experience nonlinear deformations, the possibility of fracture, which in turn result in a reduction in bearing capacity and ductility is high. Modeling fracture in structural fuses can help increase the accuracy of modeling and make the behavior of different structures more realistic. In previous sections, fracture modeling was excluded, but in this section, using two frames, one made of link beam with intermediate stiffeners and another frame made of link beam of J-LYP100 steel in the web, the occurrence of fracture and actual behavior of the two frames listed under cyclic loading have been compared.

Various studies have shown that cracking in structural steels under reversible plastic strains (in common thicknesses in structural steels) is between fatigue and ductile damage behavior [37]. According to observations, plastic strains created in structural steel under severe earthquakes are sufficient enough to cause cracks in a limited number of loading cycles (less than 20 cycles). So, often ductile fractures occur in structural steel. The fractures occurring in steel in the loading caused by the earthquake are classified as ultra low cycle fatigue.

Different studies have shown that the triaxiality ratio played an important role in the formation of ductile cracks. Stress triaxiality ratio is defined as the ratio of hydrostatic stress to von-Mises effective stress. Different researchers studied the ductile damages in metals, some of which have been mentioned below.

McClintock [38] stated that the ductile damage is caused by the expansion of voids in the material, and he also determined that the plastic strain of the fracture fits in the inverse of triaxiality by examining the cylindrical voids that are uniformly dispersed in the material. Rice and Tracey [39] observed that the ductile damage in solids was caused by the expansion and coalescence of micro-voids in the materials. In order to make the conditions more realistic than mcClintock's studies, they investigated the effect of triaxiality on the rate of expansion of a spherical void in the a uniform stress field in infinite materials with elastic perfectly plastic behavior. They finally argued that the intended spherical void changes as an exponential function of triaxiality (Eq. (30)).

$$\frac{dR}{R} = 0.283e^{\left(\frac{3}{2}\right)\left(\frac{\sigma_m}{\sigma_e}\right)} d\varepsilon_e \tag{30}$$

In 1985, Johsnon and Cook [40], experimentally and numerically studied the effect of strain rate and temperature on the fracture of metals such as copper, iron, and steel and proevided a Equation in order to predict fracture. According to studies of Kanvinde and Deierlein [41], ductile damage occurs by nucleation, growing, and coalescence of voids in places such as impurities in steel, including carbides and sulfides. And the larger the size of these impurities, the lower the stress level at which it occurs due to the less adhesion between impurities and matrix. When sufficient stress is applied to the impurities in the steel, the adhesion between these impurities and the matrix in the steel disappears or the impurities themselves are cracked and voids are created. According to the study of Kanvinde and Deierlein [41], if the radius size of the voids in the steel reaches a certain level, the fracture occurs in the sample. So, using Eq. (30) and naming materials constant as void growth index (VGI), Kanvinde and Deierlein presented the Eq. (31).

$$VGI = \frac{ln\left(\frac{R}{R_0}\right)}{C} = \int_0^{\varepsilon_P} exp(1.5T)d\varepsilon_P \tag{31}$$

In the above Equation *VGI* represents the demand for fracture in terms of the history of triaxiality (T) and the equivalent plastic strain (ε_P) in the sample. When the amount of demand for fracture exceeds the capacity of the sample, the fracture is predictable. Bao and Wierzbicki [42] observed that the mechanism of fracture was significantly dependent on the amount of triaxiality, and they also observed that most studies conducted to investigate the effect of triaxiality on fracture strain were in the range of positive triaxiality and greater than 0.33, and therefore, they investigated the effect of triaxiality on fracture strain in a wide range of triaxiality changes. For this purpose, they designed tests with triaxiality range at the fracture site between −0.33 and 0.95. Bao and Wierzbicki [42] finally, using the results of experiments with different triaxiality, experimentally presented the equivalent strain to fracture and average triaxiality according to Fig. 23.

According to Fig. 23, in negative triaxiality, shear fracture (zone 3) is created in planes with maximum shear stress. In triaxiality greater than 0.33 (zone 1), fracture caused by creation and expansion of voids and between the two mentioned conditions (zone 2), fracture has a combination of behavior of these two conditions. Bao and Wierzbicki [43], according to the tests performed and using the maximum shear stress criterion, presented their fracture criteria using only one tensile test in Eq. (32).

$$\bar{\varepsilon}_0^{pl} = \begin{cases} \infty & \eta \le -\frac{1}{3} \\ \frac{C_1}{(1+3\eta)} & -\frac{1}{3} < \eta \le 0 \\ C_1 + (C_2 - C_1)\left(\frac{\eta}{\eta_0}\right)^2 & 0 \le \eta \le \eta_0 \\ \frac{C_2\eta_0}{\eta} & \eta_0 \le \eta \end{cases} \tag{32}$$

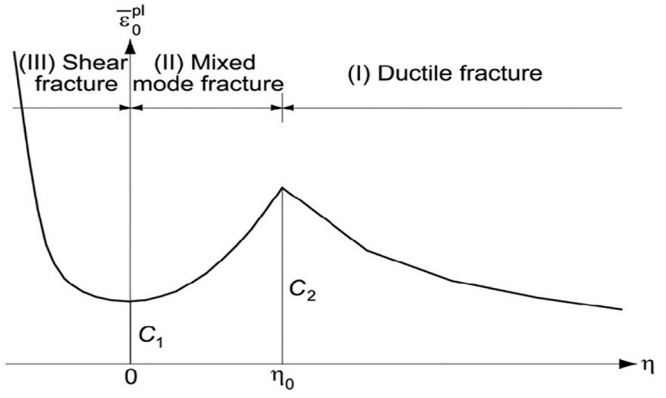

Fig. 23. The general trend of the relationship between triaxiality stress and fracture strain.

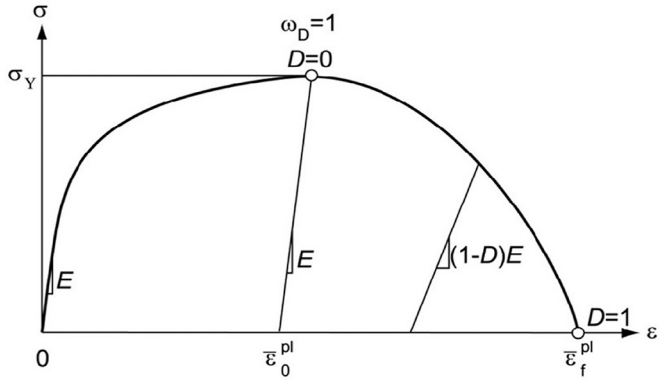

Fig. 24. Reduction of stiffness and strength after fracture begins.

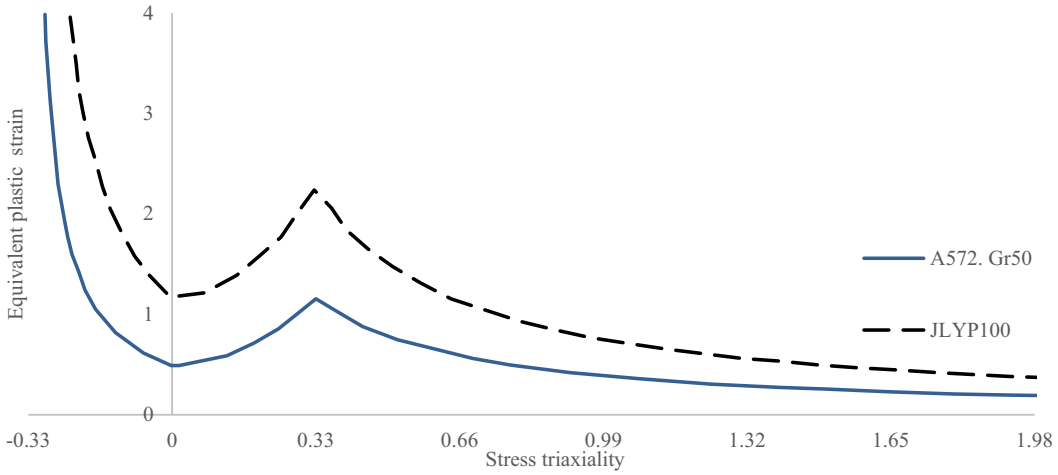

Fig. 25. Values of equivalent plastic strain to fracture with stress triaxiality change in J-LYP100 and A572 steels.

In the above Equation, C_1 and C_2 *are* equal to plastic strain of the fracture in pure shear ($\eta = 0$) and under uniaxial tension loading ($\eta = \eta_0 = 1.3$), respectively. Due to the concentration of deformation at the fracture site after the necking of the samples, the value of the C_2 coefficient, which is equal to the true strain corresponding to the fracture onset, can be obtained by the cross-section change of the sample at the site of the fracture, using the Eq. (33).

$$C_2 = -ln(1 - A_R) \tag{33}$$

Bao and Wierzbicki [43], considering the similarity of the maximum shear stress criterion with the results of the tests, presented the relationship between C_1 coefficients and C_2 in Eq. (34) in order to provide the fracture onset using only tensile test.

$$C_1 = C_2\left(\frac{\sqrt{3}}{2}\right)^{1/m} \tag{34}$$

The m parameter in the above Equation is obtained from the isotropic hardening power law in accordance with $\sigma = K_P\varepsilon^m$. The occurrence of fracture depends on the history of stress and strain values during loading. In Abaqus software, Eq. (35) is used to predict the occurrence of fracture in the material.

$$\omega_D = \int \frac{d\varepsilon^p}{\varepsilon^p_{eq}(\eta)} \tag{35}$$

ω_D is a state variable that increases with increasing the plastic strain. If the value of ω_D reaches 1 in this Equation, the fracture initiates in the intended element. With the onset of fracture in the sample, the stress and modulus of elasticity of the materials decrease so as to ultimate strain $\left(\bar{\varepsilon}^{pl}_f\right)$ the sample completely lose its strength. The evolution of stiffness and strength degradation in the element is investigated by parameter D. This parameter is defined as the ratio of the damaged surface to the total surface in a constant volume of element (Fig. 24).

In order to reduce the dependence of material behavior after the fracture onset to the size of meshing, Abaqus software uses stress-deformation relationships as an alternative to stress-strain relations. The equivalent plastic displacement ($\bar{u}^{PL}$) can be determined from the Eq. (36).

$$\bar{u}_f{}^{PL} = L_e\left(\bar{\varepsilon}^{PL}_f - \bar{\varepsilon}^{PL}_0\right) \tag{36}$$

In this Equation., L_e is the characteristic length of the element which is calculated as the second root of the area of each integration point in the two-dimensional elements and the third root of the volume of the integration point in the 3D elements.

4.3.1. *Fracture modeling in Abaqus software*

In this study, in order to model the fracture in the link beam in two frames made of ASTM A572 Gr.50 and J-LYP100 steel, Al Kajbaf et al.'s [28] studies were used. They presented the parameters related to Bao and Wierzbicki's criteria [43] for fracture modeling in two types of mentioned steel, according to Fig. 25.

In the modeling of the samples, four elements in the thickness of the flanges and the webs of the link beam have been used. Also, in order to adapt the meshing of the members according to the new geometry after the fracture, re-meshing is used using ALE Adaptive Mesh option in Abaqus software. The value of parameter $\bar{u}_f{}^{PL}$ for links with web made of ASTM A572 Gr.50 and J-LYP100 steel, according to the materials properties and mesh size is determined to be 4.57 and 6.8 mm, respectively. According to preliminary modelings, in case of welding the flanges of the link beam to the end stiffeners, due to the concentration of large amounts of plastic strain in the lower flange of the link beam, the fracture starts from these areas. The studies conducted by Berman and Bruneau [10] confirm the fracture onset from the mentioned location. For this reason, in the modeling performed in this section, the link beam

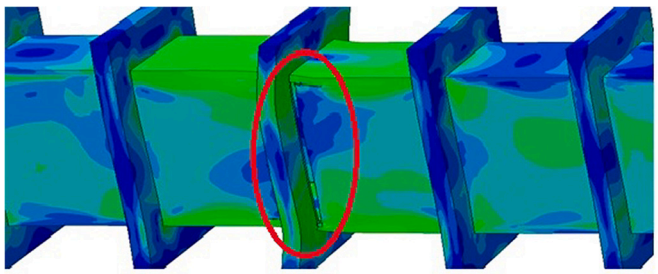

Fig. 26. The location and form of the fracture created in the link beam with the intermediate stiffeners.

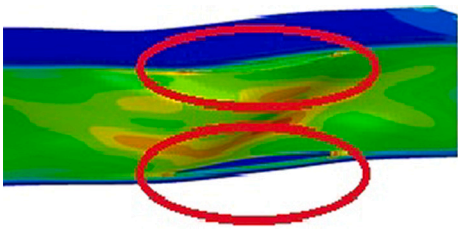

Fig. 27. The location of fracture in the link beam without intermediate stiffeners.

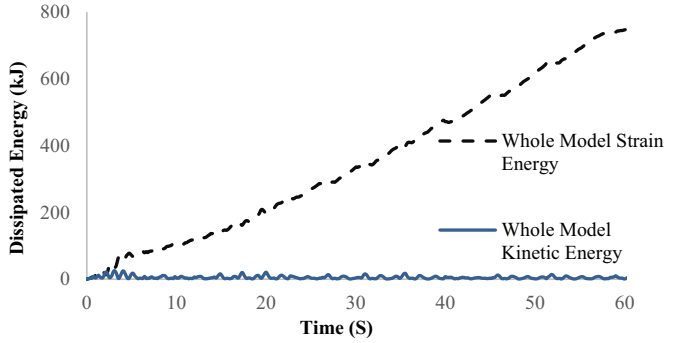

Fig. 28. Comparison of kinetic and strain energy in the frame with link beam with intermediate stiffeners.

flange is not tied to the end stiffeners. Also, in the sample with the link beam with the intermediate stiffeners, it is assumed that the stiffeners weld is cut at a distance of 2 times the thickness of the web from the outer part of the flanges. In fracture modeling, due to the removal of elements at the fracture site, the occurrence of convergence errors during analysis by static methods is probable, therefore, in this section, dynamic explicit analysis method has been used. In modeling, due to the loading of the frame in a quasi-static manner, in order to reduce the analysis time, mass scaling and time scaling methods have been used.

In the sample frame with link beam with intermediate stiffeners under cyclic loading, fracture is observed in the vicinity of the welding of the intermediate stiffener to the web in the middle of the link beam. At the time of fracture, the interstorey drift of the floor is 2% and the rotation of the link beam is 0.07 rads. So, it is clear that by modeling the fracture, the link beam sample with intermediate stiffeners is not able to achieve the target rotation of 0.08 rads. The fracture created in the link beam is shown in Fig. 26.

In the frame composed of a box link beam without intermediate transverse stiffeners and with webs made of J-LYP100 steel, fracture is created after buckling of web plate and formation of the tension field in the junction of the flange to web, with 0.13 rads link rotation and interstorey drift of 4.2%. The fracture in the sample without intermediate stiffeners, and equivalent plastic strain contour is shown in Fig. 27.

Since dynamic explicit method has been used to analyze the fracture problem in frames with box link beam under quasi-static loading, it is needed to investigate the assumption that inertia forces have no significant effect on the analysis process. To this end, kinetic energy in all frames should be less than 10% of total strain energy during loading. Kinetic energy and strain energy diagrams of the modeled frame with intermediate stiffener are shown in Fig. 28.

Similarly, for a frame made of low yield point steel, the effect of inertia forces can be ignored.

5. Conclusion

Low yield point steel has been considered as a suitable material for using in structural fuses due to low yield stress, equal modulus of elasticity with conventional steels, having high strain hardening, ductility, and high energy dissipation. Various studies have proved the advantages of using low yield point steel in structural fuses such as buckling restrained brace, shear panels, knee braces, shear walls, and link beams as a suitable method for energy dissipation. In this study, the effects of replacing webs made of ordinary steel along with intermediate stiffeners by low yield point steel without intermediate stiffeners were investigated. The main conclusions of this research are as follows:

1. The use of low yield point steel in the web of the link beam increases the net area compared to the webs made with ordinary steel and consequently the possibility of stability against local buckling increases. According to parametric modeling with full factorial method for different compactness ratios of flanges and webs, the maximum compactness ratio of web plates in box link beams made of low yield point steels in order to achieve the suitable capacity of ductility and energy dissipation, for link beams with J-LYP100 and C-LYP100 steels is 24 and 21, respectively (If the flange compactness ratio is equal or less than 25). So, using low yield point steel in the web of box link beam in order to remove intermediate stiffeners, the permissible compactness ratio of web can be increased by about 56% compared to ASTM A572 Gr.50 steel. Also, the maximum appropriate compactness ratio of the flanges for using in the shear box link beam is suggested to be $1.00\sqrt{\frac{E}{F_{yf}}}$.
2. Considering the considerable cyclic strain hardening in low yield point steels, it was found that the overstrength factor provided in different design codes are insufficient for frame design based on link beam capacity. The average values of overstrength factor for low yield point steel in the link beams made of J-LYP100 and C-LYP 100 was determined to be 4.14 and 2.58, respectively, while according to AISC 341–16, the overstrength factor value is considered to be 1.4 due to strain hardening in box link beams made of conventional steels.
3. Due to lower yield strain in low yield point steels in comparion with common structural steels, by using low yield point steel in the web of the link beam, eccentrically braced frame yields in smaller lateral displacements and as a result, energy dissipation of the link beam starts sooner in smaller lateral displacements.
4. Considerable strain hardening in low yield point steel, in addition to increasing the overstrength factor in the box link beam, increases the area under the hysteresis diagram in the non-elastic area compared to steel with an equal yield point and less strain hardening, and consequently, more energy dissipates in the link beam with low yield point steel. Using low yield point steel in the link beam, its energy dissipation can be increased by about 30%, as well as the presence of this high strain hardening in low yield point steels increases the stiffness after yielding of the link beam in the eccentrically braced frame and prevents the formation of weak or soft storeys in the structure. Using low yield point steel in the web of box link beams in multi-storey structures with eccentrically braced frame, it is possible to ensure that the link beams in all the stories are yielded and there is not any passive link beam in the structure.
5. Due to equating elastic modulus of low yield point steel with that of conventional structural steel and increasing the net area of the web using the mentioned steels in the web of the link beam, the amount of elastic stiffness of the link beam with low yield point steel in the modeled samples, are on average about 1.19 and 1.27 times the elastic stiffnes of the link beam made of conventional steel, for low yield point steel made in Japan and China, respectively. By increasing the elastic stiffness of link beam, the displacement response of eccentrically braced frame under small earthquakes, as well as the effects of secondary moments on the structure are reduced.
6. By fracture modeling of the frame with intermediate stiffeners and frame with low yield point steel J-LYP100, it was observed that the fracture occurs in the vicinity of the welding zone of the intermediate stiffeners to the web of the link beam in 0.07 rads, but in the link beam modeled with low yield point steel, with the removal of intermediate stiffeners, the fracture is not observed until 0.13 rads; So, the rotational capacity corresponding to the fracture of the link beam, is significantly increased by using low yield point steel in the web of link beam.

Authorship statement form statement

The undersigned hereby declare that:
1. the manuscript is original, does not infringe any copyright or other

proprietary rights of third parties, is not submitted for publication to another journal, and has not been previously published;

2. upon publication the undersigned author(s) transfer(s) all copyright ownership of the aforementioned manuscript to the journal Annals of Parasitology;

3. contribution of individual authors to manuscript preparation is defined in terms of the following criteria

a. Investigation;
b. Software;
c. Writing draft;
d. Original draft;
e. Conceptualization;
f. Methodology;
g. Supervision;
h. Validation;
i. Data curation;
j. Visualization;
k. Writing reviewing and editing;

Declaration of Competing Interest

The authors whose names are listed immediately below certify that they have no affiliations with or involvement in any organization or entity with any financial interest (such as employment, patent-licensing arrangements, etc.), or non-financial interest (such as personal or professional relationships, affiliations, knowledge or beliefs) in the subject matter discussed in this manuscript.

References

[1] T.T. Soong, G.F. Dargush, Passive energy dissipation and active control, Structural engineering handbook (1999) 1–28.
[2] Egor P. Popov, Kazuhiko Kasai, Michael D. Engelhardt, Advances in design of eccentrically braced frames, Earthquake Spectra 3 (1) (1987) 43–55.
[3] ANSI, AISC. "341–16, Seismic provisions for structural steel buildings 60601, 2016.
[4] Michel Bruneau, P Eng, Chia-Ming Uang, and SE Rafael Sabelli, Ductile design of steel structures, McGraw-Hill Education, 2011.
[5] Kazuhiko Kasai, Egor P. Popov, Cyclic web buckling control for shear link beams, Journal of Structural Engineering 112 (3) (1986) 505–523.
[6] Stephen P. Timoshenko, James M. Gere, Theory of elastic stability, Courier Corporation, 2009.
[7] Taichiro Okazaki, Gabriela Arce, Han-Choul Ryu, Michael D. Engelhardt, Experimental study of local buckling, overstrength, and fracture of links in eccentrically braced frames, Journal of Structural Engineering 131 (10) (2005) 1526–1535.
[8] Ming Lian, Binlin Guan, Qianqian Cheng, Hao Zhang, Su. Mingzhou, Experimental and Numerical Study of Seismic Performance of High-Strength Steel Fabricated Framed-Tube Structures with Replaceable Shear Links, Paper presented at the Structures, 2020.
[9] Peter Dusicka, Ahmad M. Itani, Ian G. Buckle, Evaluation of conventional and specialty steels in shear link hysteretic energy dissipators, in: Proceedings of 13th WCEE, Paper, no. 522, 2004.
[10] Jeffrey W. Berman, Michel Bruneau, Approaches for the seismic retrofit of braced steel bridge piers and proof-of-concept testing of an eccentrically braced frame with tubular link. No. MCEER-05-0004, Multidisciplinary Center for Earthquake Engineering Research (2005).
[11] Jeffrey W. Berman, Michel Bruneau, Further development of tubular eccentrically braced frame links for the seismic retrofit of braced steel truss bridge piers. No. MCEER-06-0006, 2006.
[12] Amin Mohebkhah, Behrouz Chegeni, Overstrength and rotation capacity for ebf links made of european Ipe sections, Thin-Walled Struct. 74 (2014) 255–260.
[13] Qianqian Cheng, Ming Lian, Su Mingzhou, Hao Zhang, Experimental and Finite Element Study of High-Strength Steel Framed-Tube Structures with Replaceable Shear Links under Cyclic Loading, Paper presented at the Structures, 2021.
[14] Eiichiro Saeki, Mitsuru Sugisawa, Tanemi Yamaguchi, Akira Wada, Mechanical properties of low yield point steels, J. Mater. Civ. Eng. 10 (3) (1998) 143–152.
[15] Gang Shi, Gao Yang, Xun Wang, Yong Zhang, Mechanical properties and constitutive models of low yield point steels, Constr. Build. Mater. 175 (2018) 570–587.
[16] T. Yamaguchi, Y. Nakata, T. Takeuchi, T. Ikebe, T. Nagao, A. Minami, T. Suzuki, Seismic control devices using low-yield-point steel; Gokuteikofukutenko, Teikofukutenko Wo Riyoshita Seishin Gijutsu No Kaihatsu, Shinnittetsu Giho (1998) 65–72.
[17] Gang Shi, Gao Yang, Xun Wang, Material properties and partial factors for resistance of low yield point steels in China, Constr. Build. Mater. 209 (2019) 295–305.
[18] Peter Dusicka, Ahmad M. Itani, Ian G. Buckle, Cyclic response of plate steels under large inelastic strains, J. Constr. Steel Res. 63 (2) (2007) 156–164.
[19] Masayoshi Nakashima, Takashi Akazawa, and Bunzo Tsuji. "strain-hardening behavior of shear panels made of low-yield steel. Ii: model.", J. Struct. Eng. 121 (12) (1995) 1750–1757.
[20] Durgesh C. Rai, Benjamin J. Wallace, Aluminium shear-links for enhanced seismic resistance, Earthquake engineering & structural dynamics 27 (4) (1998) 315–342.
[21] Li-Yan Xu, Xin Nie, Jian-Sheng Fan, Cyclic behaviour of low-yield-point steel shear panel dampers, Eng. Struct. 126 (2016) 391–404.
[22] G. De Matteis, R. Landolfo, F.M. Mazzolani, Seismic response of Mr steel frames with low-yield steel shear panels, Engineering Structures 25 (2) (2003) 155–168.
[23] Sheng-Jin Chen, Chyuan Jhang, Cyclic behavior of low yield point steel shear walls, Thin-Walled Struct. 44 (7) (2006) 730–738.
[24] Milad Bahrebar, James B.P. Lim, George Charles Clifton, Tadeh Zirakian, Amir Shahmohammadi, Mohammad Hajsadeghi, Response assessment and prediction of low yield point steel plate shear walls with curved corrugated web plates and reduced beam sections, in: Paper presented at the Structures, 2020.
[25] Peter Dusicka, Ahmad M Itani, and Ian G Buckle. "cyclic behavior of shear links of various grades of plate steel.", J. Struct. Eng. 136 (4) (2010) 370–378.
[26] Jiaojiao Wang, Yongjiu Shi, Yuanqing Wang, Constitutive model of low-yield point steel and its application in numerical simulation of buckling-restrained braces, J. Mater. Civ. Eng. 28 (3) (2016), 04015142.
[27] Cheng-Cheng Chen, Shyh-Yeang Chen, Jiunn-Jye Liaw, Application of low yield strength steel on controlled plastification ductile concentrically braced frames, Can. J. Civ. Eng. 28 (5) (2001) 823–836.
[28] Al Kajbaf, Nader Fanaie Azin, Kaveh Faraji Najarkolaie, Numerical simulation of failure in steel posttensioned connections under cyclic loading, Eng. Fail. Anal. 91 (2018) 35–57.
[29] Tadeh Zirakian, Jian Zhang, Buckling and yielding behavior of unstiffened slender, moderate, and stocky low yield point steel plates, Thin-Walled Struct. 88 (2015) 105–118.
[30] EN 1993-1-5:2005, EUROCODE 3: Design of steel structures Part 1–5: Platedstructural elements.
[31] William Prager, A new methods of analyzing stresses and strains in work hardening plastic solids, J. Appl. Mech.(ASME) 23 (1956) 493–496.
[32] Peter J. Armstrong, C.O. Frederick, A mathematical representation of the multiaxial bauschinger effect, in: Central electricity generating board [and] Berkeley Nuclear Laboratories Vol. 731, 1966.
[33] Jean-Louis Chaboche, Time-independent constitutive theories for cyclic plasticity, International journal of plasticity 2 (2) (1986) 149–188.
[34] E. Voce, A practical strain hardening function, Metallurgia 51 (1955) 219–226.
[35] Paul W. Richards, Chia-Ming Uang, Testing protocol for short links in eccentrically braced frames, Journal of Structural Engineering 132 (8) (2006) 1183–1191.
[36] Federal Emergency Management Agency, FEMA-356, Prestandard and commentary for seismic rehabilitation of buildings, Washington DC, 2000.
[37] Hitoshi Kuwamura, Transition between fatigue and ductile fracture in steel, J. Struct. Eng. 123 (7) (1997) 864–870.
[38] Frank A. McClintock, A criterion for ductile fracture by the growth of holes, 1968.
[39] J. Rice, R_, and Dennis Michael Tracey. "on the ductile enlargement of voids in triaxial stress fields*.", Journal of the Mechanics and Physics of Solids 17 (3) (1969) 201–217.
[40] Gordon R. Johnson, William H. Cook, Fracture characteristics of three metals subjected to various strains, strain rates, temperatures and pressures, Engineering fracture mechanics 21 (1) (1985) 31–48.
[41] A.M. Kanvinde, G.G. Deierlein, Finite-element simulation of ductile fracture in reduced section pull-plates using micromechanics-based fracture models, J. Struct. Eng. 133 (5) (2007) 656–664.
[42] Yingbin Bao, Tomasz Wierzbicki, On fracture locus in the equivalent strain and stress triaxiality space, Int. J. Mech. Sci. 46 (1) (2004) 81–98.
[43] H.L. Yu, D.Y. Jeong, Application of a stress triaxiality dependent fracture criterion in the finite element analysis of unnotched charpy specimens, Theor. Appl. Fract. Mech. 54 (1) (2010) 54–62.